The ORB2 RNA-binding protein represses translation of its target transcripts during the Drosophila maternal-to-zygotic transition via its functionally conserved Zinc-binding 'ZZ' domain

Timothy C.H. Low[1], Hua Luo[1], Chalini Weerasooriya[2], Sichun Lin[3], Stephane Angers[2,3], Craig A. Smibert[1,2], Howard D. Lipshitz[1]*

[1]Department of Molecular Genetics, University of Toronto, 661 University Avenue, Toronto Ontario, Canada M5G 1M1

[2]Department of Biochemistry, University of Toronto, 661 University Avenue, Toronto Ontario, Canada M5G 1M1

[3]Department of Pharmaceutical Sciences & Donnelly Centre, University of Toronto, 160 College Street, Toronto, Ontario, Canada M5S 3E1

*Author for correspondence: howard.lipshitz@utoronto.ca

Running head: ORB2 represses mRNAs during the MZT

Keywords: ORB2, Cytoplasmic Polyadenylation Element Binding Protein (CPEB), RNA-binding protein (RBP), translational regulation, post-transcriptional regulation, pre-initiation complex (PIC), embryo, maternal-to-zygotic transition (MZT), S2 cell, Cup.

ARTICLE SUMMARY

We show that Drosophila ORB2, the ortholog of the human CPEB2 RNA-binding protein, represses translation of its target mRNAs during the maternal-to-zygotic transition via its C-terminal Zinc-binding ('ZZ') domain.

ABSTRACT

RNA-binding proteins (RBPs) are key components of the post-transcriptional regulatory machinery. We show that the ORB2 RBP, the Drosophila ortholog of human Cytoplasmic Polyadenylation Element Binding Protein (hCPEB) 2-4 protein family, binds to hundreds of maternally provided mRNAs in early embryos, identify a U-rich motif enriched in ORB2's targets, and show that this motif confers ORB2 binding and repression to a luciferase reporter mRNA in S2 tissue culture cells. ORB2's target transcripts are translationally repressed and unstable during the maternal-to-zygotic transition (MZT), a developmental phase during which a large proportion of maternally provided mRNAs are repressed and cleared. We show that, when tethered to a luciferase reporter, ORB2 and hCPEB2 (but not ORB and hCPEB1) repress translation and that the C-terminal Zinc-binding ('ZZ') domain of ORB2 is necessary and sufficient for repression. ORB2 interacts with a suite of post-transcriptional regulators in early embryos; a subset of these interactions is lost upon deletion of the ZZ domain, notably with the Cup repressive complex. Analysis of the early embryo's translatome in the presence or absence of the endogenous ZZ domain, shows that ORB2's targets move onto polysomes upon ZZ domain deletion, indicating that this domain mediates translational repression of ORB2's targets during the MZT. Together, our results assign a function to the ZZ domain and support a significant role for ORB2 in post-transcriptional regulation of maternal mRNAs during the Drosophila MZT.

INTRODUCTION

Proteins belonging to the Cytoplasmic Polyadenylation Element Binding (CPEB) family are highly conserved RNA-binding proteins (RBPs) that canonically interact with U-rich motifs, known as cytoplasmic polyadenylation elements (CPEs), which are typically found in the 3′UTR of target transcripts (HAKE AND RICHTER 1994). Vertebrates have four CPEBs (CPEB1-4), while flies have two (ORB and ORB2). The CPEBs can be divided into two groups based on sequence

58 similarity: the CPEB1-like subfamily (containing vertebrate CPEB1 and its homologs, such as
59 Drosophila ORB) and the CPEB2-like subfamily (containing vertebrate CPEB2-4 and their
60 homologs, such as Drosophila ORB2) (WANG AND COOPER 2009; FERNANDEZ-MIRANDA AND
61 MENDEZ 2012; IVSHINA *et al.* 2014; DURAN-ARQUÉ *et al.* 2022).
62 CPEB proteins have been shown to function in the regulation of cytoplasmic mRNAs
63 involved in egg maturation, embryonic stem cell division, memory formation, synaptic plasticity,
64 and gametogenesis (HAKE AND RICHTER 1994; GROISMAN *et al.* 2001; KELEMAN *et al.* 2007;
65 STANDART AND MINSHALL 2008; KRÜTTNER *et al.* 2012; XU *et al.* 2012). Xenopus CPEB1, for
66 example, is a major specificity factor of an mRNA masking complex that represses translation in
67 oocytes and mediates translational activation of its target mRNAs upon egg activation (HAKE
68 AND RICHTER 1994; KIM AND RICHTER 2006).
69 *Drosophila* has a single ortholog of CPEB2-4, which is encoded by the *orb2* gene and has
70 been shown to have a role in neural development, long-term memory formation, and
71 spermatogenesis (KELEMAN *et al.* 2007; HAFER *et al.* 2011; MAJUMDAR *et al.* 2012; XU *et al.*
72 2012; KHAN *et al.* 2015; HERVÁS *et al.* 2016). The *orb2* gene encodes two protein isoforms,
73 ORB2A and ORB2B, which have 542 amino acids in common (from N-to-C): a poly-glutamine
74 (polyQ) tract, a predicted intrinsically disordered region (IDR2) that spans approximately 200
75 amino acids, the RNA-binding domain (RBD), which consists of tandem RNA recognition motif
76 (RRM) domains; and a ZZ-class Zinc-binding domain (ORB2B is diagrammed in Figure 1a).
77 ORB2A and ORB2B differ only in IDR1 at their N-termini. ORB2A-ORB2B hetero-oligomers
78 serve as translational activators whereas, in the absence of ORB2A, ORB2B does not
79 oligomerize and has been shown to repress translation of reporter transcripts *in vitro* and in S2
80 tissue culture cells (MASTUSHITA-SAKAI *et al.* 2010; KHAN *et al.* 2015; STEPIEN *et al.* 2016;
81 HERVAS *et al.* 2020).
82 All animal embryos undergo an MZT that encompasses two global processes: First, a
83 subset of maternal gene products loaded into the egg by the female parent is cleared; second, the
84 zygotic genome becomes transcriptionally active (TADROS AND LIPSHITZ 2009; VASTENHOUW *et*
85 *al.* 2019). In Drosophila embryos, the MZT is very rapid, reaching completion about 3 hours
86 after fertilization. Several RBPs have been shown to function during the first phase of the
87 Drosophila MZT (TADROS *et al.* 2007; CHEN *et al.* 2014; LAVER *et al.* 2015; HAUGEN *et al.*

88 2024) together with their co-regulatory complexes involved in translational repression (NELSON
89 *et al.* 2007; CAO *et al.* 2020) and/or mRNA degradation (SEMOTOK *et al.* 2005).
90 Here we elucidate the role of ORB2 during the Drosophila MZT and show that it
91 translationally represses hundreds of bound mRNAs through its ZZ domain. The early
92 Drosophila embryo is unusual in that only one of the two protein isoforms, ORB2B, is expressed,
93 affording us the opportunity to assess ORB2B's mechanism of action and function *in vivo* in the
94 absence of possible confounding by the presence of ORB2A. To identify protein and RNA
95 components of ORB2B-containing ribonucleoprotein complexes (RNPs) during the MZT, we
96 used a synthetic antibody to immunoprecipitate (IP) endogenously expressed ORB2-containing
97 RNPs followed by either next-generation sequencing of co-immunoprecipitated transcripts (RIP-
98 seq) or mass spectrometry of associated proteins (IP-MS). We identified over 450 transcripts
99 bound by ORB2; these are enriched for mRNAs that are translationally repressed and degraded
100 during the MZT. We also identified over 200 protein binding partners of ORB2, including
101 components of the 43S translation pre-initiation complex (PIC), the Cup-ME31B-TRAL-BEL
102 repressive complex (hereafter referred to as the Cup repressive complex). We leveraged cell
103 culture assays to map ORB2's repressive function to the C-terminal ZZ domain; showed that the
104 repressive function is conserved in its subfamily ortholog, human CPEB2 (hCPEB2) but not in
105 members of the other subfamily member, ORB or hCPEB1; and mapped the repressive function
106 to regions within the ZZ domain. We show that CRISPR deletion of the ZZ domain of
107 endogenous ORB2 results in loss of interaction with the PIC and the Cup repressive complex,
108 and derepression of ORB2's targets in early embryos, thus uncovering ORB2's post-
109 transcriptional role during the MZT.
110
111 **MATERIALS AND METHODS**
112
113 **Drosophila stocks**
114 The following *Drosophila melanogaster* stocks were used: w^{1118} and $orb^{\Delta ZZ}$. The latter
115 stock was generated for use in this study (see below). Flies were cultivated at 25°C under
116 standard laboratory conditions unless otherwise indicated.
117
118 **Generation of the CRISPR deletion of the ZZ domain at the ORB2 endogenous locus**

119 Generation of this CRISPR line was performed by Well Genetics (13F.-12, No. 93, Sec. 1,
120 Xintai 5th Rd., Xizhi Dist., New Taipei City 221416, Taiwan (R.O.C.)). The scarless PBac-
121 dsRed method was used to produce the *orb2*$^{\Delta ZZ}$ line (GRATZ *et al.* 2013; GRATZ *et al.* 2014). The
122 ZZ domain, defined as from D638 to C704 (using the numbering from the ORB2-PB isoform)
123 was targeted for deletion such that the endogenous 3'UTR was retained in its entirety. Two guide
124 RNAs (gRNAs) were used to direct CRISPR to make double-stranded cuts in the DNA
125 surrounding the mutation of interest; in our case, one gRNA was directed to the genome to a cut
126 site just after the beginning of the ZZ domain (-179 nt from STOP Codon of *orb2-RA/B/C/D/H*),
127 and the second gRNA was directed to cut +3 nt from STOP Codon. Cas9 mediates breaks in the
128 double-stranded DNA, which triggers homologous repair between the genomic locus and a donor
129 plasmid, which was co-injected with the gRNA plasmid.
130 The donor plasmid which contained the mutation of interest (a deletion of the ZZ domain,
131 which removes the genomic portion of the coding sequence after the end of the second RRM,
132 advancing the STOP codon to this point, such that this mutant protein would stop at residue
133 L637 in the PB isoform) followed by a dsRed marker flanked by Piggy Bac 5′ terminal repeats
134 (Figure S7a). The Piggy Bac transposon terminal repeats enabled this marker to be excised after
135 it had been used to screen for successful CRISPR incorporation into the genome, leaving behind
136 no trace of the marker afterwards (i.e. it is "scarless" on the genome). Flanking this dsRed
137 marker is genomic sequence that is homologous to the base genome, 1kb upstream and
138 downstream for the cut site; this provided the homology needed to facilitate homology-
139 dependent repair (HDR) between the donor plasmid and the genomic site.
140 After injections of the host w^{1118} strain (LWG182), balanced fly lines were established
141 from the resulting progeny and screened for successful integration of the mutation-containing
142 region of the donor plasmid. Successful recombination resulted in an ORB2 gene locus harboring
143 a precise deletion of the ZZ domain at the endogenous locus, marked by the expression of dsRed,
144 which was later removed from the genome using the Piggy Bac transposon machinery to excise
145 the marker by crossing them to a Piggy Bac expressing fly (BDSC #8285). This was done by
146 using primers which flanked the upstream and downstream insertion sites, where a successful
147 PCR product would only be observed when incorporation of the donor plasmid occurred at the
148 intended location in the correct orientation (Figure S7b,c).
149

150 **Synthetic antibody (Fab) expression and harvesting**

151 Phage displayed synthetic antibodies against ORB2 protein have been described previously
152 (LAVER *et al.* 2012; NA *et al.* 2016). To summarize, antigens containing amino acids 163-446
153 (numbered according to ORB2-PA isoform) were expressed and purified from *E. coli* as GST
154 fusion proteins. Synthetic antibody library F (LAVER *et al.* 2012; NA *et al.* 2016) was used in five
155 rounds of binding selection, which included negative selection to remove antibodies that bound
156 to GST, to obtain synthetic antibodies that bound to the ORB2 antigen. The two synthetic
157 antibodies used in this study were anti-ORB2 E8 and anti-hEGFR C1 (control).

158 Synthetic antibodies ('Fabs') were expressed and harvested from *E. coli* as previously
159 described (LAVER *et al.* 2012). In summary, DH5α *E. coli* was transformed with plasmid
160 containing the FLAG- and 6xHis-tagged Fab open reading frame under the control of the *lac*
161 operator. Transformed cells were used to inoculate bacterial culture using 2xYT media; the
162 inoculated culture was incubated at 37°C on rotation at 225rpm until OD595 reached 0.8. The
163 culture was then induced with isopropyl β- d-1-thiogalactopyranoside (IPTG) to drive expression
164 of the Fab and allowed to grow at 18°C overnight on rotation at 225rpm. Bacteria were pelleted
165 by centrifugation at 4°C, 4000 rpm for 30 minutes, then bacterial pellet was resuspended with B-
166 PER bacterial protein extraction reagent liquid solution (Thermo Scientific) supplemented with
167 protease inhibitors (150mM NaCl, 1mM AEBSF, 2mM Benzamidine, 2µg/mL Leupeptin,
168 2µg/mL Pepstatin) and Benzonase nuclease (2500 units/mL). Cells were allowed to lyse for 30
169 minutes at 4°C, then the lysate was cleared by centrifugation at 4°C, 15 000 rpm for 30 minutes.
170 Supernatant was collected and synthetic antibodies were purified by passing lysates through a
171 column filled with Protein A affinity gel matrix beads; the captured Fab was eluted with an acid
172 buffer containing 50mM NaH_2PO_4, 100mM H_3PO_4, and 140mM NaCl, pH to 2.8 in eight
173 fractions of 200µL each. Fab-containing fractions were pooled and dialyzed with 1L PBS at 4°C
174 for eight hours, twice. Dialyzed Fab was diluted with an equal volume of 95% glycerol 1xPBS
175 and stored at -20°C.

176

177 **Collection of embryo lysates**

178 Lysate was collected from embryos laid and aged at 25°C. Extract was prepared from
179 embryos collected 0 to 3 hours post egg-lay on apple juice agar plates, dechorionated with 100%
180 bleach for 2 minutes, washed with 0.1% Triton X-100, and disrupted by crushing in minimal

181 volume of lysis buffer consisting of 150 mM KCl, 20 mM HEPES-KOH (pH 7.4), 1 mM $MgCl_2$,
182 1 mM DTT, and protease inhibitors (1 mM AEBSF, 2 mM benzamidine, 2 µg/mL pepstatin, 2
183 µg/mL leupeptin). The lysate was cleared by centrifugation at 4°C, 13 000 RPM for 15 minutes,
184 and the supernatant was collected and either used immediately or stored at -80°C.
185
186 **RIP-seq**
187 For each replicate of RIP-seq, 1mL of 0-3 hour embryo extract (prepared as described
188 above) was supplemented with Triton X-100 to 0.1% final concentration, then diluted in an equal
189 volume of lysis buffer with 0.1% Triton X-100 and cleared again by centrifugation at 4°C, 13
190 000 RPM for 15 minutes. The supernatant was incubated for 3 to 4 hours at 4°C with end-over-
191 end rotation with 100µL of anti-FLAG M2 affinity gel beads (Sigma) which had been pre-
192 incubated at 4°C with 50µg of purified anti-ORB2 E8 Fab blocked with 5µg/µL BSA. After
193 incubation, the lysates were decanted and beads were washed four times with lysis buffer
194 supplemented with 0.1% Triton X-100 and then three times with equilibration buffer: 100 mM
195 NaCl, 100 mM HEPES-NaOH (pH 7.4), 1 mM $MgCl_2$. Fabs and associated ribonuceoprotein
196 (RNPs) were eluted from the beads with 200 µL of 200µg/µL FLAG-peptide (Sigma) suspended
197 in equilibration buffer at 4°C for 20 minutes. RNA was isolated from the eluate using TRI
198 Reagent (Sigma) according to the manufacturer's instructions.
199 RNA was prepared for sequencing using Ribo-Zero Gold rRNA depletion kit and TruSeq
200 Stranded Total RNA Library Prep Kit (Illumina) according to manufacturer's instructions.
201 Libraries were sequenced using the HiSeq 2500 System, V4 Chemistry (Illumina), with paired-
202 end reads 125nt in length. The raw data re available on GEO (accession number GSE299661).
203
204 **Computational analysis of RIP-seq data**
205 Paired-end reads obtained from the sequencing were mapped to the Drosophila
206 melanogaster transcriptome r6.23, FB2018_04 obtained from flybase.org (OZTURK-COLAK *et al.*
207 2024) using the Salmon read mapping program (PATRO *et al.* 2017). The reference transcriptome
208 was supplied as a FASTA file. The resulting quantification was then analyzed for enrichment in
209 the ORB2 IP compared to control IP using the DESeq2 software package for R (LOVE *et al.*
210 2014). Prior to formal analysis, the dataset was filtered for transcripts having >1TPM in at least
211 three of the six samples, and rlog transformation was performed to stabilize the variance. The

212 similarity between samples was calculated by determining the Poisson Distance between pairs of
213 samples using the *PoiClaClu* package in R (see Figure S1) (WHITTEN 2011).The differential
214 expression analysis was performed with the *dds* function using alpha = 0.01 cut-off for the False
215 Discovery Rate. This returned a fold enrichment for each transcript, accompanied by an adjusted
216 *P*-value. We defined an ORB2-bound RNA target as satisfying all three of the following criteria:
217 (1) it was enriched in the ORB2 IP >1.5-fold relative to Input; (2) it had an ORB2 IP/Control IP
218 ratio >1.5; (3) it had an adjusted *P*-value < 0.05. The results are presented in Figure 1 and File
219 S1.

220 For comparisons between our dataset and previously published datasets, each pairwise
221 comparison was done independently. For comparisons that required a Wilcoxon Rank Sum test,
222 for each given pair of datasets, a common background list of genes was first compiled by taking
223 the intersection between the input/background of both datasets; genes which only appeared in
224 one dataset and not the other were discarded. Then, the measurements of the remaining identified
225 genes were placed into a dataframe in which each row corresponded to one unique gene, the first
226 column contained the measurements taken from one dataset, and the second column contained
227 measurements from the other dataset. This dataframe was then used to perform a Wilcoxon Rank
228 Sum test using the wilcox.test(x, y, exact = FALSE) function in R, where x is the data in the first
229 column, y is the data in the second column. The results are shown in Figure 2.

230 For comparisons that required a Fisher's Exact Test, for each given pair of datasets a
231 common background list of genes was first compiled by taking the intersection between the
232 input/background of both datasets; genes that only appeared in one dataset and not the other were
233 discarded. Then, the remaining identified genes of interest within in each dataset were compared
234 to look for common elements; genes that were identified in both lists of interest were annotated
235 as "Overlap", whereas genes that only appeared in one list were annotated as "X Only". A
236 Fisher's Exact Test was performed by using a 2x2 contingency table, where first cell (top left)
237 contained the number of genes that did not appear in either list (equal to the total number of
238 genes in the common background minus the number of genes described in the other three cells),
239 the second cell (top right) contained number of genes that appeared only on the ORB2 list
240 (ORB2 Only), the third cell (bottom left) contained the number of genes that appeared only on
241 the other list of interest (Other Only), and the last cell (bottom right) contained the number of

242 genes appear on both lists of interest (Overlap). This contingency table was constructed and
243 evaluated using the fisher.test() function in R. The results are presented in Table 1.
244 The Gene Ontology (GO) term enrichment analysis was performed using the Functional
245 Profiling function of the web version of gProfiler2 (accessed at https://biit.cs.ut.ee/gprofiler/gost)
246 (KOLBERG *et al.* 2023). The list of ORB2 bound genes was provided to the program in the Query
247 field, and the Run Query option was selected in order to begin analysis. The results are presented
248 in Tables 2-4.
249
250 **Number of Accessible Target Sites (#ATS) *de novo* motif discovery**
251 The ORB2 motifs were identified using the #ATS model, as described (LI *et al.* 2010).
252 Briefly, the #ATS program is a *de novo* motif discovery algorithm which takes as input nucleic
253 acid sequences belonging to mRNA transcripts in two lists: a positive (in this case, the 3′UTR of
254 ORB2-bound) and negative (in this case, the 3′UTR of co-expressed and unbound) list, and
255 outputs *k*-mers that best differentiate the positive transcripts from the negative transcripts. These
256 *k*-mers are assessed based on enrichment in the positive list compared to the negative list and for
257 accessibility as predicted by computational modeling of RNA secondary structures, and assigned
258 a *P*-value (see File S2). The top five seed *k*-mers from the #ATS were combined into a consensus
259 sequence by aligning the G in the motif and converting the resulting table into a position weight
260 matrix (PWM) shown in Figure 3.
261
262 **Cell culture and transient transfection**
263 The Drosophila S2 cell line was maintained at 25°C with ExpressFive SFM (Fisher
264 Scientific) medium supplemented with 16mM L-glutamine, 100units/mL penicillin, and
265 100µg/mL streptomycin. 400µL of S2 cells at a density of 1.75×10^6 were plated and transfected
266 with a mixture of 1.5ng Firefly luciferase-6x TAR plasmid, 1.5ng Renilla luciferase plasmid,
267 20ng Tat-FLAG-effector plasmid (containing the open reading frame for either ORB2 whole
268 protein, fragments of ORB2 protein, Protein A, or GFP), 4ng of FLAG-GST, and 178.5ng pSP72
269 using 0.4µL of TransIT-Insect transection reagent (Mirius Bio) according to the manufacturer's
270 instructions. Both luciferase reporters were under the control of the metal-inducible
271 metallothionein promotor; all FLAG-tagged constructs were derived from pAc5.1/V5-His
272 plasmid (Thermo Fisher Scientific), which carries the Actin5C promotor. Luciferase expression

273 was induced 24 hours post-transfection by the addition of copper sulphate to final concentration
274 of 0.5mM. 24 hours post-induction (48 hours post-transfection), cells were harvested for
275 downstream assays.
276
277 **Luciferase Assay**
278 Cell lysate was prepared from S2 cell transient transfections by dislodging cells from the
279 surfaces of the cell culture container and transferred into conical tubes. Cells were pelleted by
280 centrifugation at 13,000 rpm at 4°C for 1 minute; the supernatant was removed, and the cell
281 pellet was resuspended in by adding 20 µL of lysis buffer (containing 1xPassive Lysis Buffer
282 [Promega], 10 mg/mL BSA, and 1 mM AEBSF). Lysis was facilitated by pipetting up and down
283 and allowing the cells to lyse at 4°C for 10 minutes. Firefly and Renilla luciferase activities were
284 measured using the Dual-Luciferase Reporter Assay system (Promega) according to
285 manufacturer's instructions.
286
287 **Reverse Transcription – Quantitative Real-time Polymerase Chain Reaction (RT-qPCR)**
288 RNA isolated from ORB2 co-immunoprecipitations was reverse transcribed into single-
289 stranded cDNA with the Superscript IV reverse transcriptase kit (Invitrogen) according to
290 manufacturer's instructions. 500ng of total RNA per sample were used to synthesize cDNA,
291 which was primed using random hexamer primers. The resulting single-stranded cDNA was
292 diluted 1:25 using RNase-free water and used to perform quantitative real-time PCR (qPCR)
293 with primers specific to the various transcripts assayed. Primers were designed using NCBU
294 Primer-BLAST to cover all isoforms produced by a gene and were required to span an exon-
295 exon junction. qPCR was performed with SensiFAST SYBR PCR mix (Bioline) following the
296 manufacturer's protocol and using 5 µL of diluted cDNA per reaction. The CFX384 Real-Time
297 System (Bio-Rad) was used to carry out the PCR reaction.
298 The results of the qPCR were analyzed using CFX Manager software (Bio-Rad). Each
299 biological replicate represented a measurement obtained for a separate embryo collection; values
300 from three technical replicates were averaged and relative gene expression was normalized to the
301 ribosomal protein-coding transcript *RpL32*. Normalized expression was presented as the average
302 of three biological replicates with error bars representing standard deviation calculated by one-
303 way ANOVA.

304

305 **Western Blots**

306 The following primary antibodies were used: mouse anti-ORB2 4GS (1:50) obtained from
307 the Developmental Studies Hybridoma Bank (https://dshb.biology.uiowa.edu/orb2-4G8) and
308 described in (HAFER *et al.* 2011), mouse M2 anti-FLAG (Sigma, 1:5,000), and mouse anti-Actin
309 (Sigma Cat#A4700, 1:10,000) which was used as a loading control.

310 Dechorionated embryos were counted, then lysed in Laemmli buffer at a concentration of 1
311 embryo/µL and boiled for 2 minutes. Proteins were resolved by SDS-PAGE and transferred to
312 PVDF membrane in the absence of SDS. The blot was blocked at room temperature with 2%
313 non-fat milk in PBST for 30 minutes and incubated with primary antibodies diluted in 2% non-
314 fat milk in PBST at 4°C overnight. After this incubation, the blot was washed 3 x 10 minutes
315 with PBST at room temperature and incubated with the appropriate HRP-conjugated secondary
316 antibodies (1:5000, Jackson ImmunoResearch) in 2% non-fat milk in PBST at room temperature
317 for 1 hour. The blot was washed 3 x 10 minutes with PBST and developed using Immobilon
318 Luminata Crescendo Western HRP substrate (Millipore), imaged using ImageLab (BioRad) and
319 band intensities were quantified using ImageLab.

320

321 **Structure Prediction with AlphaFold**

322 For structural predictions the full amino acid sequence of the ZZ domain constructs used in
323 the tethering assays (see above) was predicted using AlphaFold version 3 (JUMPER *et al.* 2021;
324 ABRAMSON *et al.* 2024). Predictions were visualized and truncated to show regions A-to-C in
325 ChimeraX version 1.9 (MENG *et al.* 2023). Structures were color-coded to depict their predicted
326 local distance difference test (pLDDT) score using the AlphaFold Error Plot tool. The results are
327 presented in Figures S4 and 5.

328

329 **Mass Spectrometry**

330 **Immunoprecipitation of ORB2 from embryo lysates with synthetic antibodies**

331 For IP-MS, 500 µL of 0-3 hour embryo extract (prepared as described above) was
332 supplemented with Triton X-100 to 0.1% final concentration, then diluted in an equal volume of
333 lysis buffer with 0.1% Triton X-100 and cleared again by centrifugation at 4°C, 13 000 RPM for
334 15 minutes. The supernatant was incubated for 3 to 4 hours at 4°C with end-over-end rotation

335 with 100µL of anti-FLAG M2 affinity gel beads (Sigma) which had been pre-incubated at 4°C
336 with 50µg of purified anti-ORB2 E8 Fab blocked with 5µg/µL BSA. After incubation, the lysates
337 were decanted and beads were washed twice with lysis buffer supplemented with 0.1% Triton X-
338 100, then another twice with lysis buffer without Triton X-100; beads were transferred into a
339 new tube and washed another twice with lysis buffer without Triton X-100. Fabs and associated
340 proteins were eluted by tryptic digest: Beads were resuspended in 200 µL of 50mM ammonium
341 bicarbonate pH 8 supplemented with 2 µg of MS-grade trypsin and incubated at room
342 temperature overnight with end-over-end rotation. The digested peptides were collected and a
343 second elution with 200 µL of 50mM ammonium bicarbonate was performed at room
344 temperature for 30 minutes. The two fractions were pooled, flash frozen with dry ice, dehydrated
345 in a rotary evaporator for 8 hours, then stored at -20°C.
346
347 **Liquid chromatography and mass spectrometry**
348 For liquid chromatography (LC) the following solvents were used: Solvent A (0.1%
349 (vol/vol) formic acid) and Solvent B (0.1% (vol/vol) formic acid/90% (vol/vol) acetonitrile). The
350 LC parameters were set using an Easy-nLC 1200 instrument. Peptides were loaded and separated
351 on a nanoViper trap column (75µm x 2 cm), Acclaim PepMap 100 (C18, 3µm, 100 Å, Thermo
352 Scientific, cat. no. 164946), and EASY-Spray analytical column (75µm x 50cm) Acclaim
353 PepMap RSLC (C18, 2µm, 100Å, Thermo Scientific) using a flow rate of 225nL/minute.
354 Tandem MS was performed using the Q Exactive HF-Orbitrap mass spectrometer (Thermo
355 Scientific), as previously described (LIU *et al.* 2014; JIANG *et al.* 2015; CHIU *et al.* 2016). The
356 parameters for acquisition were 1 MS scan (50 ms; mass range, 390 to 1800) at a resolution of
357 60,000K, followed by up to 20 MS/MS scans (50 ms each) at a resolution of 15,000 and an AGC
358 target of 1x105. Candidate ions with charge states +2 to +7 were isolated using a window of 1.4
359 amu with a 5s dynamic exclusion window.
360
361 **Data processing and analysis**
362 Four biological replicates were performed, both in the presence or absence of RNase A.
363 The ProHits software package was used to perform Significance Analysis of INTeractome
364 (SAINT) in order to identify ORB2-interacting proteins (LIU *et al.* 2010; CHOI *et al.* 2012; LIU *et*
365 *al.* 2012). Proteins with associated peptide counts were filtered through the Trans Proteomic

366 Pipeline (TPP) for iProphet probability > 0.95 and number of unique peptides ≥2. SAINT
367 express analysis was performed on the ProHits interface with only Drosophila detected proteins
368 (selected options: number of compressed controls = 3, burn-in period, nburn = 2000; iterations,
369 niter = 5000, lowMode = 1; minFold = 1; normalize = 1; nCompressBaits = 3). This analysis
370 determined the probability of interaction for each identified prey protein. Proteins with AvgP
371 score ≥ 0.95 and BFDR ≤ 0.01 were defined as ORB2-ineracting proteins. Raw data are available
372 at MassIVE MSV000098275. The results are presented in File S3.
373 To perform network analysis on the list of identified protein interactors, we used the
374 GeneMANIA application (v3.5.2) (WARDE-FARLEY *et al.* 2010; FRANZ *et al.* 2018) with the
375 Cytoscape network visualization program (v3.9.1) (SHANNON *et al.* 2003; MONTOJO *et al.* 2010).
376 Data resulting from the IP-MS was imported to Cytoscape in table form. The interaction network
377 was produced by performing a Network Search on the list of proteins using the *Drosophila*
378 *melanogaster* database of GeneMANIA. The nodes of this network were then annotated
379 according to the number of spectral counts detected in our IP-MS and the edges were annotated
380 with known physical and genetic interactions reported in the GeneMANIA database. The results
381 are presented in Figure 5.
382
383 **Embryo Sample Collection for *orb*$^{\Delta ZZ}$ Time-course and Polysome Gradient RNA-seq**
384 Embryos were collected from *orb2*$^{\Delta ZZ}$ and *w*^{1118} (pre-injected control, LWG182) strains at
385 1-hour intervals post-egglay (0-1 hour, 1-2 hour, 2-3 hour), dechorionated with ice cold 100%
386 bleach for 2 minutes, washed with 0.1% Triton X-100, and disrupted by crushing using 0.5 g
387 embryos per mL of either lysis buffer (150 mM KCl, 20 mM HEPES-KOH (pH 7.4), 1 mM
388 MgCl2, 1 mM DTT, 1 mM AEBSF, 2 mM benzamidine, 2 µg/mL pepstatin, 2 µg/mL leupeptin)
389 or polysome lysis buffer (7.5 mM MgCl2, 500 mM NaCl, 25 mM Tris (pH 7.5), 1 mM DTT, 1
390 mM AEBSF, 2 µg/mL leupeptin, 2 mM benzamidine, 2 µg/mL pepstatin A, 2 mg/mL heparin,
391 0.5 mg/mL cycloheximide). The lysate with lysis buffer was cleared by centrifugation at 4°C, 13
392 000 RPM for 15 minutes, TRIzol (Invitrogen) was added to the supernatant which used
393 immediately for RNA extraction or stored at -80°C. The lysate with polysome lysis buffer was
394 either used immediately for polysome gradient processing or stored at -80°C.
395
396 **Polysome Gradients**

397 The polysome gradient protocol was adapted from our published method with
398 modifications (CHEN *et al.* 2014). Lysed samples were diluted 1 in 10 in polysome lysis buffer
399 and 20% Triton X-100 was added to a final concentration of 1%, centrifuged at 6,000xg for 10
400 minutes and the resulting supernatant was diluted in polysome lysis buffer supplemented with
401 1% Triton X-100 to an A_{260} of 12.5. A 5 ml 15% to 45% linear sucrose gradient in 7.5 mM
402 $MgCl_2$, 500 mM NaCl, 50 mM Tris pH 7.5 was produced using a BioComp Model 117 Gradient
403 Mate gradient maker (Biocomp, Fredericton, New Brunswick, Canada) using a rotation angle of
404 86 degrees and a rotation speed of 25 for 51 seconds. After chilling the polysome gradient at 4ºC
405 for 1 hour, 200 µL of diluted embryo extract was loaded onto the top of the gradient, which was
406 then spun at 36,000 rpm in a Beckman SW50.1 rotor for 2.5 hours. 400 µL fractions (hand
407 fractionated) were collected, and A_{260} absorbance was measured using a Nanodrop (Thermo
408 Fisher Scientific). We added 20% SDS, 0.5 M EDTA and 20 mg/ml proteinase K to final
409 concentrations of 0.8%, 0.01 M and 0.128 mg/ml, respectively, and then incubated the fractions
410 for 30 minutes at 37ºC. 2.5 µL GlycoBlue (15 mg/mL, ThermoFisher) following which 2.5x
411 volume ethanol was added to each fraction and precipitated overnight. The resulting pellet was
412 washed with 75% ethanol and resuspended in phenol-saturated water.
413 The fractions were then separated into three pools: Pool 1 contained the (top) fractions 1-3,
414 pool 2 contained fractions 4-6, pool 3 contained fractions 7-13. Following two phenol-
415 chloroform extractions, the aqueous phase of each pool was collected with Invitrogen
416 Phasemaker Tubes (Fisher A33248) following the manufacturer's protocol. The samples were
417 precipitated by the addition of 7.5 M LiCl to a final concentration of 3.75 M followed by an
418 overnight incubation at -20°C. The pellets were washed with 70% ethanol and resuspended in
419 water.
420 RNA purification was performed using 2.2× volume NEBNext RNA Sample Purification
421 Beads (NEBNext Ultra II DNA Library Prep with Sample Purification Beads, E7767L)
422 following the manufacturer's protocol. RNA concentration was assessed with the Qubit RNA HS
423 Assay Kit (Thermo Fisher) and Agilent bioanalyzer at The Centre for Applied Genomics
424 (TCAG), The Hospital for Sick Children, Toronto, ON, Canada.
425
426 **rRNA Depletion, Library Preparation and RNA-seq for Time-course and Polysome**
427 **Gradient RNA-seq**

428 For the RNA-seq time-course rRNA depletion was performed as previously described
429 (HAUGEN *et al.* 2024). For polysome gradient RNA-seq, rRNA depletion was performed using
430 the QIAseq FastSelect rRNA Fly Kit (QIAGEN, Cat# 33326). Library preparation for RNA-seq
431 was conducted using the NEBNext Ultra II Directional RNA Library Prep Kit for Illumina, and
432 sequencing was performed on an Illumina NovaSeq 6000 (PE150) at the Next Generation
433 Sequencing Facility, The Centre for Applied Genomics (TCAG), The Hospital for Sick Children,
434 Toronto, ON, Canada.
435
436 **Computational Analysis of Time-course and Polysome Gradient RNA-seq Data**
437
438 **RNA-seq data processing pipeline:**
439 Adapter trimming and quality control used Trim Galore (Version 0.6.5)
440 [https://github.com/FelixKrueger/TrimGalore]. rRNA and 'unwanted' RNA removal used
441 SortMeRNA (version 2.1) (KOPYLOVA *et al.* 2012), filtering against Drosophila melanogaster
442 7SLRNA, rRNA, pseudogene-rRNA, tRNA, mtRNA and other species' rRNA databases.
443 Transcriptome alignment was carried out with Salmon (Version 1.9.1) (PATRO *et al.* 2017) in
444 mapping-based mode using FlyBase release 6.23 transcriptome RNA (FB2018_04) (OZTURK-
445 COLAK *et al.* 2024). Full decoy indexing was applied following the salmon website instructions
446 [https://salmon.readthedocs.io/en/latest/salmon.html].
447
448 **Differential gene expression analysis:**
449 Differential expression analysis used the R package tximeta (version 1.20.3) (LOVE *et al.*
450 2020) and Deseq2 (version 1.42.1) (LOVE *et al.* 2014) in R (version 4.3.2). For the *orb2*$^{\Delta ZZ}$ and
451 wild type time-course total RNA-seq, reads from each time point were normalized using the
452 DESeq2 package. For the *orb*2$^{\Delta ZZ}$ and wild type polysome gradient RNA-seq time-courses, reads
453 of each time point of *orb2*$^{\Delta ZZ}$ and wild type pool 1 and pool 3 RNA were normalized using the
454 DESeq2 package. For each gene, the mean of normalized counts per pool was computed at each
455 time point and genotype. The 'Translation Index' of each mRNA was calculated as the ratio =
456 mean normalized counts of pool 3 /mean normalized counts of pool 1. Normalized counts were
457 used for statistical analysis by the Wilcoxon Rank Sum Test and data were visualized with
458 ggplot2 in R. Raw data are available at GEO for the RNA-seq timecourse and polysome gradient

timecourse with accession numbers GSE299140 and GSE299019, respectively. The results are presented in Figure 6 and Files S5 and 6.

RESULTS

ORB2 binds to over 450 targets in the early Drosophila embryo

To identify RNA transcripts that are bound by ORB2B (hereafter referred to as ORB2), we used our previously produced Fab against an antigen N-terminal to the RRMs (Figure 1a) (LAVER *et al.* 2012; NA *et al.* 2016). We used this antibody to perform RNA-coimmunoprecipitation (RIP) of endogenously expressed ORB2 from embryo extracts prepared from 0-3 hour old embryos produced by w^{1118} females. We enriched for mRNA in the sample by rRNA depletion, generated randomly primed cDNA libraries from the resulting samples, and we identified co-purifying RNAs by next-generation RNA sequencing (see Materials and Methods). As a negative control, we performed parallel RIPs using a control synthetic antibody, C1, as described previously (LAVER *et al.* 2015; LAVER *et al.* 2020; HAUGEN *et al.* 2024). Input samples from the same extracts were also sequenced. We performed three biological replicates for each of these three conditions, for a total of nine cDNA libraries.

To identify ORB2-bound target genes, we mapped the sequence reads to the Drosophila transcriptome using Salmon read alignment software, and analyzed the results with the DESeq2 software package as described in Materials and Methods (LOVE *et al.* 2014; PATRO *et al.* 2017). We identified 462 genes whose transcripts were bound by ORB2 (Figure 1b and File S1). ORB2-bound transcripts were significantly less abundant than co-expressed unbound transcripts (Figure 1b). RIP-RT-qPCR verified several of the bound and unbound targets (Figure 1c).

While ours is the first identification of ORB2 targets in embryos, there are previously published target lists from other tissues or cells. For example, ORB2-bound transcripts were identified in a CLIP experiment derived from ORB2 overexpression in S2 cells (STEPIEN *et al.* 2016). Of the 462 ORB2 targets on our list, 298 were identified in their CLIP-seq background set of which they identified 113 as targets (Fisher's exact $P = 6.52\text{x}10^{-7}$, Odds Ratio = 1.88). We also examined the overlap of our targets with a list of ORB2-associated transcripts obtained by performing RIP-seq on Drosophila head extracts (KOZLOV *et al.* 2023). 336 genes in our target gene list overlapped with theirs (Fisher's exact $P < 10^{-15}$, Odds Ratio = 5.00).

489 The strong overlap between our ORB2 targets and previously reported targets from other
490 cell types/tissues verifies that our list is enriched for true ORB2 interactors.
491
492 **ORB2 targets are translationally repressed and degraded during the MZT**
493 To assess the post-transcriptional fate of ORB2-bound transcripts in the early Drosophila
494 embryo we utilized three previously published datasets that scored each transcript's translational
495 status, poly(A) tail length, and abundance during the MZT.
496 Two studies measured Translation Efficiency (TE), calculated from ribosome profiling,
497 during the MZT (DUNN *et al.* 2013; EICHHORN *et al.* 2016). At all three timepoints during the
498 MZT that were studied, ORB2-bound transcripts had a significantly lower TE compared to co-
499 expressed, unbound transcripts (Figure 2a-c). A third study measured Translation Index (TI),
500 calculated as the ratio of that transcript's abundance in polysome fractions of a sucrose gradient
501 compared to its abundance in non-polysomal fractions (CHEN *et al.* 2014). ORB2-bound
502 transcripts had a significantly lower TI than co-expressed unbound transcripts (Figure 2d).
503 We next assessed changes in poly(A) tail length and abundance for ORB2 targets between
504 the 0-1 hour timepoint and the 2-3 hour timepoint, which had been measured in parallel to TE
505 (EICHHORN *et al.* 2016). ORB2 targets underwent a significantly greater decrease in poly(A) tail
506 length and abundance than co-expressed, unbound transcripts (Figure 2e,f). We also examined
507 previously published lists of transcripts that are degraded during the MZT (Table 1). ORB2
508 targets overlapped significantly with transcripts identified to be unstable in activated eggs
509 (TADROS *et al.* 2007) (Fisher's Exact $P = 2.2 \times 10^{-16}$, odds ratio 3.85). In addition, ORB2 targets
510 were significantly enriched for genes that are degraded during the MZT (THOMSEN *et al.* 2010):
511 (Class III and V; respectively, Fisher's Exact $P = 0.02$, odds ratio 1.54 and Fisher's Exact $P =$
512 2.2×10^{-16}, odds ratio 2.54) and significantly depleted for transcripts that are stable (Class I;
513 Fisher's Exact $P = 2.2 \times 10^{-16}$, odds ratio 0.23).
514 We conclude that ORB2's target mRNAs are enriched for transcripts that are
515 translationally repressed, deadenylated and degraded during the MZT.
516
517 **ORB2 targets are enriched for roles in gamete generation, gene regulation, and**
518 **development**

519 Having assessed the post-transcriptional fate of ORB2's targets, we next asked whether
520 these targets were enriched for particular molecular, cellular or biological functions by
521 performing Gene Ontology (GO) term analysis using the gProfiler2 tool (GENE ONTOLOGY *et al.*
522 2023; KOLBERG *et al.* 2023) (Tables 2-4).
523 The top GO terms under the Molecular Function category (Table 2) were dominated by
524 molecular binding functions; 'mRNA 3′UTR binding', and 'mRNA regulatory element binding'
525 were among the top ten results. Genes belonging to these terms included *orb2* itself as well as
526 *patronin, piwi,* and *bru1*. Other top terms included 'translation regulator activity' and 'translation
527 repressor activity'; genes belonging to these terms included *orb2* itself, *orb, pum, fmr1, sxl, heph,*
528 and *eIF4E-HP*. In the Biological Process category (Table 3), ORB2 targets were enriched for
529 terms related to regulation and development, such as 'anatomical structure development', 'cell
530 differentiation', and 'regulation of metabolic process'. ORB2 targets were also enriched for
531 terms related to gametogenesis, including 'gamete generation', 'oogenesis', and 'germ cell
532 development'. Genes related to these terms included *pum, rbfox1, piwi, heph, bru1, sxl,* and *mei-*
533 *P26*. Enrichment for GO terms related to gametogenesis in ORB2 targets is consistent with
534 previously reported functions for ORB2 in, for example, regulation of spermatogenesis (XU *et al.*
535 2012; GILMUTDINOV *et al.* 2021). The Cellular Component category (Table 4) was dominated by
536 terms that included 'ribonucleoprotein granule', 'P granule', 'pole plasm', and 'germ plasm'.
537 Genes related to these terms included *larp, tud, osk, tapas, ago1,* and *dcr-2*.
538 Many of the genes listed under enriched GO terms are previously identified ORB2 targets
539 (e.g., *orb2* itself, *ago1*, *bru1, dcr-2*, *eIF4E-HP*, *fmr1*, *heph*, *orb, pum, rbfox1, unr*)
540 (MASTUSHITA-SAKAI *et al.* 2010; XU *et al.* 2012; STEPIEN *et al.* 2016; KOZLOV *et al.* 2021) while
541 others are previously unidentified players in the same enriched function or process (e.g., *imp and*
542 *piwi*). Enrichment for mRNAs encoding known post-transcriptional regulators suggests that
543 ORB2 may play a key role in the cross-regulatory network that controls the MZT, a function that
544 is supported by our subsequent analyses reported below. The fact that ORB2 binds to and
545 potentially regulates mRNAs that encode other post-transcriptional regulators is also consistent
546 with a previous study in S2 cells showing that RNP complexes tend to be enriched for mRNAs
547 encoding post-transcriptional regulators (STOIBER *et al.* 2015).
548
549 **ORB2-bound transcripts are enriched for a U-rich motif**

550 CPEB-family proteins are known to bind to U-rich elements, typically located in the
551 3′UTR of their mRNA targets (HAKE AND RICHTER 1994; DE MOOR AND RICHTER 1999; STEPIEN
552 *et al.* 2016). To predict *cis*-elements recognized by ORB2 from our *in vivo* RIP-seq results, we
553 used our algorithm, Number of Accessible Target Sites (#ATS), which performs *de novo* motif
554 discovery given a target set and a co-expressed non-target set of transcripts (LI *et al.* 2010).
555 Using our input RNA-seq data, we identified the most abundant transcript isoform from each
556 expressed gene in the early embryo and then compared the 3′UTR sequences of ORB2 targets to
557 those of non-targets. The #ATS program identified a list of 6-mers enriched in ORB2 target
558 sequences relative to non-targets; these 6-mers were then combined into a consensus motif
559 (Figure 3a, File S2), which will henceforth be referred to as an ORB2-recognition element
560 (ORE). The ORE, NUUGUWU (where W = A or U) has similarities to published binding motifs:
561 KUUUKKK (where K = G or U) identified by an *in vitro* binding assay (RAY *et al.* 2013);
562 UUUU$(A)_{1\text{-}3}$U and UUUUGU identified in S2 cells (STEPIEN *et al.* 2016); UUUURU (where R =
563 A or G) in brain extracts (MASTUSHITA-SAKAI *et al.* 2010).
564 The *de novo* discovery of a U-rich ORE enriched in ORB2-bound RNAs in the early
565 embryo and its similarity to ORB2 motifs previously identified using a variety of methods
566 supports the conclusion that our list of targets is enriched for transcripts directly bound by
567 ORB2.
568
569 **The ORE directs ORB2 binding to and repression of a luciferase reporter mRNA in S2**
570 **cells**
571 To validate the biological activity of the ORE identified by #ATS, we used a luciferase
572 reporter assay in Drosophila S2 cells to measure ORB2 binding and ORB2-mediated regulation.
573 In the assay, firefly (FLuc) reporters harboured six copies in the 3′UTR of either a representative
574 ORE (UUUUGUU) or a mutated ORE (UUAUCUC) (the reporter is schematized in Figure 3b).
575 Each of these reporters was individually expressed in S2 cells together with either a control
576 protein (GFP), full-length ORB2 protein, or an ORB2 protein lacking its RBD (ORB2ΔRRM).
577 An unregulated Renilla luciferase (Rluc) reporter was co-transfected with all samples, allowing
578 us to normalize Fluc mRNA and protein levels.
579 ORB2 RIP followed by RT-qPCR confirmed that the reporters carrying the wild-type
580 OREs, but not the mutant OREs, were enriched in ORB2 IPs, compared to IPs of the

581 ORB2ΔRRM protein (Figure 3c). Furthermore, significant ORB2-mediated repression of the
582 reporter was seen when ORB2 protein was expressed together with a reporter construct carrying
583 wild-type OREs (Figure 3d). When either the OREs were mutated or the RRM was deleted, no
584 repression was observed (Figure 3d) despite the fact that ORB2ΔRRM protein was expressed at
585 higher levels than full-length ORB2 (Figure S2).
586 We conclude that ORB2 binds to OREs and that this binding confers repression on a
587 reporter RNA. The extent of repression we observed is similar to that previously reported for
588 ORB2B in similar reporter assays in S2 cells (STEPIEN *et al.* 2016).
589
590 **The C-terminal Zinc-binding ('ZZ') domain of ORB2/hCPEB2 but not ORB/hCPEB1**
591 **represses a luciferase reporter mRNA in S2 cells**
592 To identify domains of ORB2 necessary and sufficient for repression we used a luciferase
593 reporter tethering assay in S2 cells. We transfected a plasmid construct that would express a
594 protein containing the BIV-Tat RNA-binding domain fused to all or part of the ORB2 protein.
595 This fusion protein is recruited to six tandem repeats of the trans-activating response (TAR)
596 element (to which BIV-Tat binds) located in the 3′UTR of a co-transfected firefly luciferase
597 reporter (schematised in Figure 4a). Tethering of full-length ORB2B protein produced significant
598 repression relative to a tethered GFP control (Figure 4b); the extent of repression was consistent
599 with previously published data for ORB2 in S2 cells (STEPIEN *et al.* 2016). Tethering of ORB2
600 protein did not affect steady-state reporter RNA levels (Figure 4c).
601 To map regions of ORB2 that mediate repression, we fused the BIV-tat domain to
602 fragments of the ORB2 protein and assessed whether any individual region was capable of
603 repressing luciferase expression. We divided the ORB2 protein into five fragments: IDR1, the
604 polyQ region, IDR2, the RBD, and the ZZ domain (Figures 1a and 4b,c). There was no
605 significant effect on the expression of luciferase after tethering of IDR1, polyQ, or IDR2 (Figure
606 4b and see Figure S3A for western blot of expression of each fragment). The RBD and the ZZ
607 domain conferred repression (Figure 4b). We note that the RBD was over-expressed relative to
608 the other fragments; however, the ZZ domain produced very strong (~three-fold) repression
609 despite being expressed at a comparatively low level (Figure S3a). To determine whether the ZZ
610 domain was also necessary for repression, we tethered an ORB2 protein construct lacking the ZZ
611 domain (ORB2ΔZZ) to the luciferase reporter and found that it was unable to repress luciferase

612 expression, despite ORB2ΔZZ retaining the RBD and being expressed at higher levels than full-
613 length ORB2 (Figure 4b, Figure S3b). Because luciferase mRNA levels were not significantly
614 different from controls in either the ZZ sufficiency or the ZZ necessity experiments (Figure 4c,
615 ZZ and ORB2ΔZZ), ZZ domain mediated repression can be attributed largely to effects on
616 translation rather than RNA stability. We conclude that the ZZ domain of ORB2 is both
617 necessary and sufficient to confer translational repression when tethered to a reporter mRNA.
618 Finally, to assess possible conservation of function, we also tethered the ZZ domains of
619 ORB, hCPEB1 and hCPEB2. The hCPEB2 ZZ domain conferred significant repression, whereas
620 the ORB ZZ and hCPEB1 ZZ domain were unable to repress (Figure 4e; western blot is shown
621 in Figure S3c). We conclude that the repressive function of the ZZ domain is conserved between
622 ORB2 and its human ortholog, hCPEB2, while it is not conserved in ORB or hCPEB1. We note
623 that the ZZ domains of hCPEB3 and hCPEB4 are ≥ 90% identical to the hCPEB2 ZZ domain.
624 This suggests that, although not tested here, the hCPEB3 and hCPEB4 ZZ domains likely also
625 function in translational repression.
626
627 **Regions within the ORB2 ZZ domain are sufficient to confer repression**
628 To map regions of the ORB2 ZZ domain sufficient for repression, we first compared the
629 sequences of the ZZ domains of ORB, ORB2, hCPEB1 and hCPEB2. There is high level of
630 sequence identity between the ORB2 ZZ domain and that of hCPEB2 (81.3% amino acid
631 identity, Figure 4d). In contrast, the ZZ domain of ORB2 and ORB, exhibit only 35.6% sequence
632 identity and hCPEB1 has only 28.5% amino acid identity to ORB2 (Figure 4d). We then
633 considered the predicted structures of these domains (Figure S4). An NMR structure of the
634 hCPEB1 ZZ domain showed it consists of a rubredoxin (Rd) turn, followed by a beta hairpin,
635 and a short alpha helix (MERKEL *et al.* 2013). Predictions of the structures of the ORB, ORB2
636 and hCPEB2 ZZ domains using Alphafold 3 (ABRAMSON *et al.* 2024) showed a similar
637 arrangement. Indeed, Alphafold3 prediction of the ORB ZZ structure was virtually identical to
638 that of the NMR structure of the hCPEB1 ZZ domain (Figure S4a). Similarly, the predictions of
639 the ORB2 and hCPEB2 ZZ structures were very similar to one another (Figure S4a). Finally, an
640 overlap of the ORB and ORB2 ZZ domain structures showed that the only difference was the
641 length of the Rd turn (Figure S4b).

642 To map regions within the ORB2 ZZ domain sufficient for repression we focused on the 46
643 amino acids beginning two amino acids before the first zinc-coordinating residue (at Q640) and
644 ending at the C-terminal zinc-coordinating residue (H685). We asked whether we could
645 transform the non-repressive ORB ZZ domain into a repressive one by substituting the Rd turn
646 ('A', Q640 to P656), the beta hairpin ('B', F657-Y668), and/or the alpha helix ('C', C669 to
647 H685) regions of the ORB2 ZZ domain into the corresponding portion of the ORB ZZ domain
648 and assessing their function using the tethering assay. Importantly, AlphaFold3 did not predict
649 any disruptions in the folding of the chimeric proteins when the ORB ZZ domain carried one of
650 these ORB2 regions (Figure S5).
651 When the entire 46 amino acid region was substituted from the ORB2 ZZ domain into the
652 ORB ZZ domain (ORB ZZ-$A^2B^2C^2$, where the superscript '2' refers to ORB2 and superscript '1'
653 refers to ORB), the chimeric construct produced significant repression relative to the GFP
654 control (Figure 4f). Region A (ORB ZZ-$A^2B^1C^1$) and region C (ORB ZZ-$A^1B^1C^2$) produced
655 significant repression whereas region B (ORB ZZ-$A^1B^2C^1$) did not (Figure 4f; western blots are
656 shown in Figure S6).
657 We conclude that regions A and C of the ORB2 ZZ domain are each sufficient to convert
658 the ORB ZZ domain into a repressor.
659
660 **ORB2 interacts with translational repressors and the 43S translation preinitiation complex**
661 **in early embryos**
662 We next turned to proteomic strategies to identify protein partners of ORB2 in early
663 embryos. We immunoprecipitated endogenous ORB2 from extracts prepared from embryos
664 produced by w^{1118} females, both in the presence and absence of RNase A, in biological
665 quadruplicates, using the same synthetic antibody used above to identify ORB2 target RNAs.
666 Co-purifying proteins were identified by mass spectrometry followed by Significance Analysis
667 of INTeractome (SAINT), which assigns confidence scores to protein-protein interactions based
668 on proteomic data (CHOI *et al.* 2012). We defined a protein interactor of ORB2 as any protein
669 that was significantly enriched in ORB2 immunoprecipitates compared to parallel purifications
670 using our negative control Fab, C1, with a SAINT (AvgP) score ≥ 0.95 and a BFDR < 0.01 (File
671 S3).

672 We identified 212 interactors of ORB2 in the absence of RNase A and 106 interactors in
673 the presence of RNase A, the latter representing RNA-independent interactions; 85 were in
674 common (File S3). The interactors largely fell into two distinct groups: The first consisted of
675 RBPs known to negatively regulate target stability and/or translation, including AGO1, AGO2,
676 PUM, and RBFOX1, as well as the Cup repressive complex (Cup, ME31B, TRAL, BEL)
677 (GOTZE *et al.* 2017) (Figure 5a, File S3). All components of the Cup repressive complex
678 copurified in the presence of RNase, consistent with an RNA-independent interaction with
679 ORB2. The second group consisted of translation-initiation factors, notably the components of
680 the 43S preinitiation complex (PIC): all eIF3 and eIF2 subunits, eIF1 and -1A, and eIF5A; most
681 (13/20) were RNA-independent interactors, including 11/14 detected eIF3 subunits (Figure 5b
682 and File S3).
683 We note that a subset of ORB2's protein interactors were also identified as mRNA targets
684 in our RIP-seq experiments (File S4). This result is consistent with an earlier study of RBP
685 mRNA targets and protein interactors carried out in S2 cells, which showed that RNP complexes
686 are enriched for both mRNAs and their encoded proteins involved in RNA binding and post-
687 transcriptional regulation (STOIBER *et al.* 2015).
688 Co-purification of ORB2 with negative regulators of mRNA stability and translation is
689 consistent with our analyses of the post-transcriptional fate of ORB2 targets during the MZT
690 (repressed and unstable; Figure 2) and our reporter experiments in S2 cells (repressed, Figures 3
691 and 4). In the Discussion, we consider possible reasons for the lack of an effect on stability in S2
692 cells as well as possible implications of the PIC interaction.
693
694 **The ORB2 ZZ domain is required for interaction with the 43S PIC and the Cup repressive**
695 **complex**
696 The experiments described above showed that the ZZ domain of ORB2 is necessary and
697 sufficient for translational repression in our S2-cell tethering assay; therefore, we assessed
698 whether this domain is important for association with ORB2's identified binding partners in
699 early embryos. To generate an endogenous deletion of the ZZ domain, we used a scarless dsRed
700 CRISPR method to remove all amino acids from ORB2 D638 to the C-terminus at C704,
701 inclusive, leaving the endogenous 3′UTR intact (see Figure 4d, Materials and Methods, Figure
702 S7) (GRATZ *et al.* 2013; GRATZ *et al.* 2014). The mutant fly lines resulting from the excision will

703 henceforth be referred to as *orb2*$^{\Delta ZZ}$. Western blots on whole-fly extract showed that ORB2ΔZZ
704 was expressed at higher levels than full-length ORB2 in the pre-CRISPRed *w*^{1118} wild-type
705 control flies (Figure S7d) and a similar result was obtained for 0-3 hour embryos (Figure S8a).
706 We confirmed by RIP-RT-qPCR that deletion of the ZZ domain did not significantly affect
707 ORB2ΔZZ's ability to bind to several of its RNA targets in embryos (Figure S8b).
708 Immunopurification of ORB2ΔZZ protein from 0-3 hour embryos produced by *orb2*$^{\Delta ZZ}$
709 homozygous females followed by mass spectrometry identified 91 high-confidence protein
710 interactors in the absence and 48 in the presence of RNase A, of which 43 overlapped (File S3).
711 When the union of these interactors (96 proteins) was compared to the union of full-length
712 ORB2 IP-MS interactors (233 proteins), we found that 65 overlapped, including several
713 translational repressors such as PUM and RBFOX1 (File S3). Strikingly, interactions with all
714 components of the PIC and the Cup repressive complex were lost upon deletion of the ZZ
715 domain.
716 We conclude that the ORB2 ZZ domain is required for interaction between ORB2 and the
717 43S PIC as well as the Cup repressive complex, but that additional repressors retain interaction
718 with ORB2 in the absence of its ZZ domain.
719
720 **The ZZ domain is necessary for translational repression of ORB2 targets in the early**
721 **embryo**
722 Since our experiments in S2 cells showed that the ZZ domain is necessary for ORB2-
723 mediated translational repression, and our IP-MS results indicated that ORB2 loses interactions
724 with the Cup repressive complex when the ZZ domain is deleted, we next asked whether deletion
725 of the ZZ domain had consequences for post-transcriptional regulation of ORB2's target mRNAs
726 during the MZT.
727 First, we assessed whether ORB2's targets, which are enriched for maternal transcripts that
728 are deadenylated and degraded during the MZT (see Figure 2e,f), were stabilized in ORB2ΔZZ
729 mutant embryos. We collected embryo extracts from embryos laid by control or *orb2*$^{\Delta ZZ}$ females
730 at 0-1, 1-2 and 2-3 hours after egg lay and carried out RNA-seq followed by analysis using
731 DEseq2. We compared the expression level of targets and co-expressed non-targets across this
732 time course and found that, at all three stages, there was no significant difference in expression
733 level between control versus ORB2ΔZZ embryos for either target or non-target transcripts

734 (Figure 6a and File S5). These results suggest that, while ORB2 binds to unstable mRNAs, it
735 does not induce their degradation or, alternatively, that ORB2 may direct destabilization of its
736 targets during the MZT in a ZZ domain-independent mechanism.
737 Second, we assessed whether ORB2's targets, which are enriched for transcripts with
738 significantly lower TE and TI than co-expressed non-targets (see Figure 2a-d), underwent an
739 increase in polysome association in ORB2ΔZZ embryos. We collected embryo extracts from
740 embryos laid by control or *orb2*$^{\Delta ZZ}$ females at 0-1, 1-2 and 2-3 hours after egg lay, then ran
741 polysome gradients followed by RNA-seq of pooled polysome fractions and pooled 'free' (non-
742 polysome-associated) fractions. For each gene, we calculated the ratio of RNA in the polysome
743 fractions to that in the free fractions (see Materials and Methods); if translational repression were
744 relieved upon deletion of the ZZ domain then this ratio would increase (i.e., transcripts would
745 move onto polysomes).We found that, in ORB2ΔZZ embryos, ORB2 targets shifted onto
746 polysomes at the first timepoint (0-1 hour) whereas non-targets did not (Figure 6b and File S6).
747 We conclude that the ZZ domain of ORB2 mediates translational repression of ORB2
748 targets at the beginning of the MZT. At subsequent timepoints (1-2 and 2-3 hours), there was no
749 significant difference in polysome association of ORB2 targets in ORB2ΔZZ embryos versus
750 controls; possible reasons will be considered in the Discussion.
751
752 **DISCUSSION**
753 In this study, we identified hundreds of RNA targets and protein partners of the Drosophila
754 ORB2 protein in the early embryo. ORB2's targets are enriched for translationally repressed
755 mRNAs that are degraded during the MZT. These targets are enriched for a U-rich motif that
756 directs binding and repression of a reporter in S2 cells. Repression by ORB2 is mediated by the
757 ZZ domain, a function that is conserved in hCPEB2. Deletion of the ZZ domain from the
758 endogenous ORB2 gene results in loss of physical interaction with the Cup repressive complex
759 and derepression of ORB2's mRNA targets in the early embryo.
760
761 **A conserved role for the ORB2/hCPEB2 ZZ domain in mediating translational repression**
762 Structural analysis of the ZZ domain of hCPEB1 has implicated it in protein-protein
763 interaction (MERKEL *et al.* 2013; STEPIEN *et al.* 2016), consistent with earlier studies on, for
764 example, the ZZ domain of CREB-binding protein (LEGGE *et al.* 2004). Our identification of

765 multiple proteins that depend *in vivo* on the ZZ domain for interaction with ORB2 are consistent
766 with a major role in recruiting co-regulators to target transcripts. Our data showing that deletion
767 of the ZZ domain does not affect RNA binding are consistent with a previous study (STEPIEN *et*
768 *al.* 2016). The fact that, in our S2 cell tethering assay, the ZZ domain is necessary and sufficient
769 for repression permitted us to assess evolutionary conservation of this role as well as to map
770 regions of the ZZ domain that implement this function.
771 Interestingly, we found that the repressive function of the entire ZZ domain is conserved
772 between ORB2 and hCPEB2 but not with ORB and hCPEB1. Swapping regions from ORB2 into
773 ORB identified which of these are sufficient for repression. Notably, the Rd turn at the N-
774 terminus ('A', Q640 to P656) and the α-helix at the C-terminus ('C', C669 to H685) were
775 sufficient to transform the ORB ZZ domain into a repressor. The ZZ domains of hCPEB3 and 4
776 show ≥ 90% amino acid identity to hCPEB2, with 16 of the 17 residues of region A and 12 of
777 the 13 residues of region C identical between hCPEB2-4. As such, it is quite likely that the ZZ
778 domains of hCPEB3 and 4 are also capable of repressing target mRNA translation via regions A
779 and C.
780 That fact that region A or C of ORB2's ZZ domain are each sufficient to convert the ORB
781 ZZ domain into a translational repressor indicates that they can function independent of one
782 another, perhaps by binding to different co-repressors. Future work aimed at identifying the
783 ORB2 binding partners that interact with regions A and/or C should provide insights into the
784 molecular mechanisms that underlie ZZ domain function.
785
786 **Regulation of post-transcriptional processes during the MZT**
787 Our analyses of the post-transcriptional fate of ORB2's targets during the MZT indicate
788 that they are enriched for transcripts that are translationally repressed and degraded. Consistent
789 with this outcome, multiple negative regulators of mRNA translation and stability copurify with
790 ORB2 in early embryos; most of these copurify in the presence of RNase, consistent with an
791 RNA-independent interaction with ORB2. Several of the regulators that interact in an RNA-
792 independent manner require the ZZ domain for interaction (notably, the Cup complex
793 components – Cup, TRAL, ME31B and BEL) while others interact both in the presence and
794 absence of the ZZ domain (e.g., PUM, FMR1, RBFOX1).

795 The S2 cell reporter assay showed that, while full-length ORB2 and its isolated ZZ domain
796 are both able to repress translation, they did not affect steady-state RNA levels. The simplest
797 explanation for this difference between S2 cells and embryos is that key factors that direct
798 degradation in embryos may not be present or may be expressed at low levels in S2 cells. For
799 example, RBFOX1, which we identified as an ORB2-interactor by IP-MS in early embryos, is
800 expressed at low levels in S2 cells according to RNA-seq data (CHERBAS *et al.* 2011). At present
801 our results indicating a role for ORB2 in degrading mRNAs in the embryo are correlative;
802 experiments to assess whether ORB2 directly triggers degradation of target mRNAs during the
803 MZT and the role of ORB2-interactors in this regulation awaits further investigation. What is
804 clear is that if ORB2 does play such a role, it does not require the ZZ domain.
805 We have shown that the ZZ domain is necessary and sufficient for translational repression
806 of reporters in S2 cells and is required to repress ORB2's *in vivo* targets in 0-1 hour embryos.
807 That the Cup complex is expressed in both S2 cells and embryos, that ZZ domain deletion results
808 in loss of Cup complex interaction with ORB2 in embryos, and that ORB2's targets in embryos
809 lose repression when the ZZ domain is deleted from endogenous ORB2, are all consistent with
810 the hypothesis that ORB2-dependent repression is mediated by the Cup complex. The Cup
811 complex prevents interaction of eIF4G with eIF4E, thus abrogating translation initiation
812 (WILHELM *et al.* 2003; NAKAMURA *et al.* 2004; NELSON *et al.* 2004); consistent with this role, we
813 note that, while eIF4E was present in our ORB2 IP-MS data, eIF4G was absent. Previous
814 studies have shown that the Cup complex is brought to mRNAs by BRU1 in oocytes and by
815 SMG in embryos (WILHELM *et al.* 2003; NAKAMURA *et al.* 2004; NELSON *et al.* 2004). ORB2
816 would represent a third RBP that recruits this complex for repression, in this case early in the
817 MZT.
818 The Cup complex has been shown to be cleared by the CTLH E3 ligase part-way through
819 the MZT (CAO *et al.* 2020; ZAVORTINK *et al.* 2020), consistent with the ZZ domain's repressive
820 role in the early but not late MZT. However, ORB2's targets are repressed at both 0-1 hour
821 (when the Cup complex is present) and at 2-3 hours (after the Cup complex has been cleared);
822 furthermore, ORB2's targets are deadenylated and degraded between 0-1 and 2-3 hours, but
823 deletion of the ZZ domain has no effect on their clearance. These data suggest that additional
824 regulators may function either independent of or together with ORB2 to direct these processes; if
825 the latter, they would interact with domains of ORB2 distinct from the ZZ domain. PUM, FMR1

826 and RBFOX1 are present throughout the MZT (CASAS-VILA *et al.* 2017; CAO *et al.* 2020) and
827 we have shown here that their interaction with ORB2 is both RNA-independent and ZZ-domain
828 independent, making them candidates for implementing these roles.
829
830 **The mystery of PIC interaction**
831 Unexpectedly, we identified the 43S PIC as a major interactor of ORB2 via its ZZ domain.
832 An essential component of the PIC is the eIF3 complex (its subunits are encoded by 14 genes in
833 *Drosophila*), which is a highly regulated component of translation initiation (HARRIS *et al.* 2006;
834 CHIU *et al.* 2010; CATE 2017). Several of the mammalian eIF3 subunits have been shown to have
835 RNA-binding ability (LEE *et al.* 2015; LEE *et al.* 2016) and to mediate distinct regulatory
836 outcomes (PESTOVA *et al.* 1998; PESTOVA AND HELLEN 1999; HUI *et al.* 2003; HUI *et al.* 2005;
837 MARTINEAU *et al.* 2008; LEE *et al.* 2010; MARTINEAU *et al.* 2014).
838 At this time we do not have data that provide insights into the functional consequences of
839 ORB2's interaction with the PIC. ORB2's interaction with the PIC's eIF3 subunits is RNA-
840 independent, consistent with direct interaction with one or more of these subunits. One
841 possibility that we considered is that ORB2 may sequester the PIC, thus reducing translation
842 overall. However, in such a model, one would expect a global increase in translation upon loss of
843 PIC interaction rather than what we observed in ORB2ΔZZ embryos, which is an increase in
844 polysome association of ORB2's targets but no change in non-targets. An alternative hypothesis
845 is that ORB2-dependent binding to the PIC on target transcripts has a negative effect on
846 translation either in addition to or in concert with the Cup repressive complex. Indeed, a
847 speculative model might be that ORB2 binding to the 3′UTR and interaction with PIC at the
848 5′UTR might repress translation initiation by interfering with PIC function. The mechanistic and
849 functional consequences of ORB2-PIC interaction will be a fruitful area for future study.
850
851 **Data Availability**
852 Drosophila strains are available upon request. Raw data for RIP-seq, RNA-seq and IP-MS
853 are available at GEO (GSE299661 for RIP-seq, GSE299140 for RNA-seq time-course,
854 GSE299019 for polysome gradient seq) and at MassIVE (MSV000098275 for IP-MS). The
855 authors affirm that all of the other data necessary for confirming the conclusions of the article are
856 present within the article, figures, tables and supplementary files.

Acknowledgements

We thank Kun Nie for assisting with the *de novo* motif discovery using #ATS and Dr. Dorothy Lerit for feedback on a draft of this manuscript.

Funding

This research was supported by grants from the Canadian Institutes of Health Research PJT-159702 (HDL), PJT-190124 (HDL) and PJT-159494 (CAS). TCHL was supported in part by a Canada Graduate Scholarship (CGS-M) and a University of Toronto Open Fellowship; CW was supported in part by a University of Toronto Open Fellowship. Molecular graphics and analyses were performed with UCSF ChimeraX, developed by the Resource for Biocomputing, Visualization, and Informatics at the University of California, San Francisco, with support from National Institutes of Health R01-GM129325 and the Office of Cyber Infrastructure and Computational Biology, National Institute of Allergy and Infectious Diseases.

Conflicts of Interest

The authors declare that they have no conflicts of interest.

875 **LITERATURE CITED**

876

877 Abramson, J., J. Adler, J. Dunger, R. Evans, T. Green *et al.*, 2024 Accurate structure prediction
878 of biomolecular interactions with AlphaFold 3. Nature 630**:** 493-500.
879 Cao, W. X., S. Kabelitz, M. Gupta, E. Yeung, S. Lin *et al.*, 2020 Precise Temporal Regulation of
880 Post-transcriptional Repressors Is Required for an Orderly Drosophila Maternal-to-
881 Zygotic Transition. Cell Rep 31**:** 107783.
882 Casas-Vila, N., A. Bluhm, S. Sayols, N. Dinges, M. Dejung *et al.*, 2017 The developmental
883 proteome of Drosophila melanogaster. Genome Res 27**:** 1273-1285.
884 Cate, J. H., 2017 Human eIF3: from 'blobology' to biological insight. Philos Trans R Soc Lond B
885 Biol Sci 372.
886 Chen, L., J. G. Dumelie, X. Li, M. H. Cheng, Z. Yang *et al.*, 2014 Global regulation of mRNA
887 translation and stability in the early Drosophila embryo by the Smaug RNA-binding
888 protein. Genome Biol 15**:** R4.
889 Cherbas, L., A. Willingham, D. Zhang, L. Yang, Y. Zou *et al.*, 2011 The transcriptional diversity
890 of 25 Drosophila cell lines. Genome Res 21**:** 301-314.
891 Chiu, C. W. N., C. Monat, M. Robitaille, M. Lacomme, A. M. Daulat *et al.*, 2016 SAPCD2
892 Controls Spindle Orientation and Asymmetric Divisions by Negatively Regulating the
893 Galphai-LGN-NuMA Ternary Complex. Dev Cell 36**:** 50-62.
894 Chiu, W. L., S. Wagner, A. Herrmannová, L. Burela, F. Zhang *et al.*, 2010 The C-terminal
895 region of eukaryotic translation initiation factor 3a (eIF3a) promotes mRNA recruitment,
896 scanning, and, together with eIF3j and the eIF3b RNA recognition motif, selection of
897 AUG start codons. Mol Cell Biol 30**:** 4415-4434.
898 Choi, H., G. Liu, D. Mellacheruvu, M. Tyers, A. C. Gingras *et al.*, 2012 Analyzing protein-
899 protein interactions from affinity purification-mass spectrometry data with SAINT. Curr
900 Protoc Bioinformatics Chapter 8**:** Unit8.15.
901 de Moor, C. H., and J. D. Richter, 1999 Cytoplasmic polyadenylation elements mediate masking
902 and unmasking of cyclin B1 mRNA. EMBO J 18**:** 2294-2303.
903 Dunn, J. G., C. K. Foo, N. G. Belletier, E. R. Gavis and J. S. Weissman, 2013 Ribosome
904 profiling reveals pervasive and regulated stop codon readthrough in Drosophila
905 melanogaster. Elife 2**:** e01179.
906 Duran-Arqué, B., M. Cañete, C. L. Castellazzi, A. Bartomeu, A. Ferrer-Caelles *et al.*, 2022
907 Comparative analyses of vertebrate CPEB proteins define two subfamilies with
908 coordinated yet distinct functions in post-transcriptional gene regulation. Genome Biol
909 23**:** 192.
910 Eichhorn, S. W., A. O. Subtelny, I. Kronja, J. C. Kwasnieski, T. L. Orr-Weaver *et al.*, 2016
911 mRNA poly(A)-tail changes specified by deadenylation broadly reshape translation in
912 Drosophila oocytes and early embryos. Elife 5.
913 Fernandez-Miranda, G., and R. Mendez, 2012 The CPEB-family of proteins, translational
914 control in senescence and cancer. Ageing Res Rev 11**:** 460-472.
915 Franz, M., H. Rodriguez, C. Lopes, K. Zuberi, J. Montojo *et al.*, 2018 GeneMANIA update
916 2018. Nucleic Acids Res 46**:** W60-W64.
917 Gene Ontology, C., S. A. Aleksander, J. Balhoff, S. Carbon, J. M. Cherry *et al.*, 2023 The Gene
918 Ontology knowledgebase in 2023. Genetics 224.

919 Gilmutdinov, R., E. N. Kozlov, K. V. Yakovlev, L. V. Olenina, A. A. Kotov *et al.*, 2021 The
920 3'UTR of the Drosophila CPEB translation factor gene orb2 plays a crucial role in
921 spermatogenesis. Development 148.
922 Gotze, M., J. Dufourt, C. Ihling, C. Rammelt, S. Pierson *et al.*, 2017 Translational repression of
923 the Drosophila nanos mRNA involves the RNA helicase Belle and RNA coating by
924 Me31B and Trailer hitch. RNA 23**:** 1552-1568.
925 Gratz, S. J., A. M. Cummings, J. N. Nguyen, D. C. Hamm, L. K. Donohue *et al.*, 2013 Genome
926 engineering of Drosophila with the CRISPR RNA-guided Cas9 nuclease. Genetics 194**:**
927 1029-1035.
928 Gratz, S. J., F. P. Ukken, C. D. Rubinstein, G. Thiede, L. K. Donohue *et al.*, 2014 Highly
929 specific and efficient CRISPR/Cas9-catalyzed homology-directed repair in Drosophila.
930 Genetics 196**:** 961-971.
931 Groisman, I., Y. S. Huang, R. Mendez, Q. Cao and J. D. Richter, 2001 Translational control of
932 embryonic cell division by CPEB and maskin. Cold Spring Harb Symp Quant Biol 66**:**
933 345-351.
934 Hafer, N., S. Xu, K. M. Bhat and P. Schedl, 2011 The Drosophila CPEB protein Orb2 has a
935 novel expression pattern and is important for asymmetric cell division and nervous
936 system function. Genetics 189**:** 907-921.
937 Hake, L. E., and J. D. Richter, 1994 CPEB is a specificity factor that mediates cytoplasmic
938 polyadenylation during Xenopus oocyte maturation. Cell 79**:** 617-627.
939 Harris, T. E., A. Chi, J. Shabanowitz, D. F. Hunt, R. E. Rhoads *et al.*, 2006 mTOR-dependent
940 stimulation of the association of eIF4G and eIF3 by insulin. EMBO J 25**:** 1659-1668.
941 Haugen, R. J., C. Barnier, N. D. Elrod, H. Luo, M. K. Jensen *et al.*, 2024 Regulation of the
942 Drosophila transcriptome by Pumilio and the CCR4-NOT deadenylase complex. RNA
943 30**:** 866-890.
944 Hervás, R., L. Li, A. Majumdar, M. e. C. Fernández-Ramírez, J. R. Unruh *et al.*, 2016 Molecular
945 Basis of Orb2 Amyloidogenesis and Blockade of Memory Consolidation. PLoS Biol 14**:**
946 e1002361.
947 Hervas, R., M. J. Rau, Y. Park, W. Zhang, A. G. Murzin *et al.*, 2020 Cryo-EM structure of a
948 neuronal functional amyloid implicated in memory persistence in *Drosophila*. Science
949 367**:** 1230-1234.
950 Hui, D. J., C. R. Bhasker, W. C. Merrick and G. C. Sen, 2003 Viral stress-inducible protein p56
951 inhibits translation by blocking the interaction of eIF3 with the ternary complex
952 eIF2.GTP.Met-tRNAi. J Biol Chem 278**:** 39477-39482.
953 Hui, D. J., F. Terenzi, W. C. Merrick and G. C. Sen, 2005 Mouse p56 blocks a distinct function
954 of eukaryotic initiation factor 3 in translation initiation. J Biol Chem 280**:** 3433-3440.
955 Ivshina, M., P. Lasko and J. D. Richter, 2014 Cytoplasmic polyadenylation element binding
956 proteins in development, health, and disease. Annu Rev Cell Dev Biol 30**:** 393-415.
957 Jiang, T., R. F. McKinley, M. A. McGill, S. Angers and T. J. Harris, 2015 A Par-1-Par-3-
958 Centrosome Cell Polarity Pathway and Its Tuning for Isotropic Cell Adhesion. Curr Biol
959 25**:** 2701-2708.
960 Jumper, J., R. Evans, A. Pritzel, T. Green, M. Figurnov *et al.*, 2021 Applying and improving
961 AlphaFold at CASP14. Proteins 89**:** 1711-1721.
962 Keleman, K., S. Krüttner, M. Alenius and B. J. Dickson, 2007 Function of the Drosophila CPEB
963 protein Orb2 in long-term courtship memory. Nat Neurosci 10**:** 1587-1593.

964 Khan, M. R., L. Li, C. Pérez-Sánchez, A. Saraf, L. Florens *et al.*, 2015 Amyloidogenic
965 Oligomerization Transforms Drosophila Orb2 from a Translation Repressor to an
966 Activator. Cell 163**:** 1468-1483.
967 Kim, J. H., and J. D. Richter, 2006 Opposing polymerase-deadenylase activities regulate
968 cytoplasmic polyadenylation. Mol Cell 24**:** 173-183.
969 Kolberg, L., U. Raudvere, I. Kuzmin, P. Adler, J. Vilo *et al.*, 2023 g:Profiler-interoperable web
970 service for functional enrichment analysis and gene identifier mapping (2023 update).
971 Nucleic Acids Res 51**:** W207-W212.
972 Kopylova, E., L. Noe and H. Touzet, 2012 SortMeRNA: fast and accurate filtering of ribosomal
973 RNAs in metatranscriptomic data. Bioinformatics 28**:** 3211-3217.
974 Kozlov, E., Y. V. Shidlovskii, R. Gilmutdinov, P. Schedl and M. Zhukova, 2021 The role of
975 CPEB family proteins in the nervous system function in the norm and pathology. Cell
976 Biosci 11**:** 64.
977 Kozlov, E. N., E. V. Tokmatcheva, A. M. Khrustaleva, E. S. Grebenshchikov, R. V. Deev *et al.*,
978 2023 Long-Term Memory Formation in Drosophila Depends on the 3'UTR of CPEB
979 Gene orb2. Cells 12.
980 Krüttner, S., B. Stepien, J. N. Noordermeer, M. A. Mommaas, K. Mechtler *et al.*, 2012
981 Drosophila CPEB Orb2A mediates memory independent of Its RNA-binding domain.
982 Neuron 76**:** 383-395.
983 Laver, J. D., K. Ancevicius, P. Sollazzo, J. T. Westwood, S. S. Sidhu *et al.*, 2012 Synthetic
984 antibodies as tools to probe RNA-binding protein function. Mol Biosyst 8**:** 1650-1657.
985 Laver, J. D., X. Li, D. Ray, K. B. Cook, N. A. Hahn *et al.*, 2015 Brain tumor is a sequence-
986 specific RNA-binding protein that directs maternal mRNA clearance during the
987 Drosophila maternal-to-zygotic transition. Genome Biol 16**:** 94.
988 Laver, J. D., J. Ly, A. K. Winn, A. Karaiskakis, S. Lin *et al.*, 2020 The RNA-Binding Protein
989 Rasputin/G3BP Enhances the Stability and Translation of Its Target mRNAs. Cell Rep
990 30**:** 3353-3367 e3357.
991 Lee, A. S., P. J. Kranzusch and J. H. Cate, 2015 eIF3 targets cell-proliferation messenger RNAs
992 for translational activation or repression. Nature 522**:** 111-114.
993 Lee, A. S., P. J. Kranzusch, J. A. Doudna and J. H. Cate, 2016 eIF3d is an mRNA cap-binding
994 protein that is required for specialized translation initiation. Nature 536**:** 96-99.
995 Lee, J. P., A. Brauweiler, M. Rudolph, J. E. Hooper, H. A. Drabkin *et al.*, 2010 The TRC8
996 ubiquitin ligase is sterol regulated and interacts with lipid and protein biosynthetic
997 pathways. Mol Cancer Res 8**:** 93-106.
998 Legge, G. B., M. A. Martinez-Yamout, D. M. Hambly, T. Trinh, B. M. Lee *et al.*, 2004 ZZ
999 domain of CBP: an unusual zinc finger fold in a protein interaction module. J Mol Biol
1000 343**:** 1081-1093.
1001 Li, X., G. Quon, H. D. Lipshitz and Q. Morris, 2010 Predicting in vivo binding sites of RNA-
1002 binding proteins using mRNA secondary structure. RNA 16**:** 1096-1107.
1003 Liu, G., J. Zhang, H. Choi, J. P. Lambert, T. Srikumar *et al.*, 2012 Using ProHits to store,
1004 annotate, and analyze affinity purification-mass spectrometry (AP-MS) data. Curr Protoc
1005 Bioinformatics Chapter 8**:** 8.16.11-18.16.32.
1006 Liu, G., J. Zhang, B. Larsen, C. Stark, A. Breitkreutz *et al.*, 2010 ProHits: integrated software for
1007 mass spectrometry-based interaction proteomics. Nat Biotechnol 28**:** 1015-1017.

1008 Liu, Y. C., A. L. Couzens, A. R. Deshwar, B. M.-C. LD, X. Zhang *et al.*, 2014 The PPFIA1-
1009 PP2A protein complex promotes trafficking of Kif7 to the ciliary tip and Hedgehog
1010 signaling. Sci Signal 7**:** ra117.
1011 Love, M. I., W. Huber and S. Anders, 2014 Moderated estimation of fold change and dispersion
1012 for RNA-seq data with DESeq2. Genome Biol 15**:** 550.
1013 Love, M. I., C. Soneson, P. F. Hickey, L. K. Johnson, N. T. Pierce *et al.*, 2020 Tximeta:
1014 Reference sequence checksums for provenance identification in RNA-seq. PLoS Comput
1015 Biol 16**:** e1007664.
1016 Majumdar, A., W. C. Cesario, E. White-Grindley, H. Jiang, F. Ren *et al.*, 2012 Critical role of
1017 amyloid-like oligomers of Drosophila Orb2 in the persistence of memory. Cell 148**:** 515-
1018 529.
1019 Martineau, Y., M. C. Derry, X. Wang, A. Yanagiya, J. J. Berlanga *et al.*, 2008 Poly(A)-binding
1020 protein-interacting protein 1 binds to eukaryotic translation initiation factor 3 to stimulate
1021 translation. Mol Cell Biol 28**:** 6658-6667.
1022 Martineau, Y., X. Wang, T. Alain, E. Petroulakis, D. Shahbazian *et al.*, 2014 Control of Paip1-
1023 eukayrotic translation initiation factor 3 interaction by amino acids through S6 kinase.
1024 Mol Cell Biol 34**:** 1046-1053.
1025 Mastushita-Sakai, T., E. White-Grindley, J. Samuelson, C. Seidel and K. Si, 2010 Drosophila
1026 Orb2 targets genes involved in neuronal growth, synapse formation, and protein turnover.
1027 Proc Natl Acad Sci U S A 107**:** 11987-11992.
1028 Meng, E. C., T. D. Goddard, E. F. Pettersen, G. S. Couch, Z. J. Pearson *et al.*, 2023 UCSF
1029 ChimeraX: Tools for structure building and analysis. Protein Sci 32**:** e4792.
1030 Merkel, D. J., S. B. Wells, B. C. Hilburn, F. Elazzouzi, G. C. Pérez-Alvarado *et al.*, 2013 The C-
1031 terminal region of cytoplasmic polyadenylation element binding protein is a ZZ domain
1032 with potential for protein-protein interactions. J Mol Biol 425**:** 2015-2026.
1033 Montojo, J., K. Zuberi, H. Rodriguez, F. Kazi, G. Wright *et al.*, 2010 GeneMANIA Cytoscape
1034 plugin: fast gene function predictions on the desktop. Bioinformatics 26**:** 2927-2928.
1035 Na, H., J. D. Laver, J. Jeon, F. Singh, K. Ancevicius *et al.*, 2016 A high-throughput pipeline for
1036 the production of synthetic antibodies for analysis of ribonucleoprotein complexes. RNA
1037 22**:** 636-655.
1038 Nakamura, A., K. Sato and K. Hanyu-Nakamura, 2004 Drosophila cup is an eIF4E binding
1039 protein that associates with Bruno and regulates oskar mRNA translation in oogenesis.
1040 Dev Cell 6**:** 69-78.
1041 Nelson, M. R., A. M. Leidal and C. A. Smibert, 2004 Drosophila Cup is an eIF4E-binding
1042 protein that functions in Smaug-mediated translational repression. The EMBO journal
1043 23**:** 150-159.
1044 Nelson, M. R., H. Luo, H. K. Vari, B. J. Cox, A. J. Simmonds *et al.*, 2007 A multiprotein
1045 complex that mediates translational enhancement in Drosophila. J Biol Chem 282**:**
1046 34031-34038.
1047 Ozturk-Colak, A., S. J. Marygold, G. Antonazzo, H. Attrill, D. Goutte-Gattat *et al.*, 2024
1048 FlyBase: updates to the Drosophila genes and genomes database. Genetics 227.
1049 Patro, R., G. Duggal, M. I. Love, R. A. Irizarry and C. Kingsford, 2017 Salmon provides fast and
1050 bias-aware quantification of transcript expression. Nat Methods 14**:** 417-419.
1051 Pestova, T. V., and C. U. Hellen, 1999 Internal initiation of translation of bovine viral diarrhea
1052 virus RNA. Virology 258**:** 249-256.

1053 Pestova, T. V., I. N. Shatsky, S. P. Fletcher, R. J. Jackson and C. U. Hellen, 1998 A prokaryotic-
1054 like mode of cytoplasmic eukaryotic ribosome binding to the initiation codon during
1055 internal translation initiation of hepatitis C and classical swine fever virus RNAs. Genes
1056 Dev 12**:** 67-83.
1057 Ray, D., H. Kazan, K. B. Cook, M. T. Weirauch, H. S. Najafabadi *et al.*, 2013 A compendium of
1058 RNA-binding motifs for decoding gene regulation. Nature 499**:** 172-177.
1059 Semotok, J. L., R. L. Cooperstock, B. D. Pinder, H. K. Vari, H. D. Lipshitz *et al.*, 2005 Smaug
1060 recruits the CCR4/POP2/NOT deadenylase complex to trigger maternal transcript
1061 localization in the early Drosophila embryo. Curr Biol 15**:** 284-294.
1062 Shannon, P., A. Markiel, O. Ozier, N. S. Baliga, J. T. Wang *et al.*, 2003 Cytoscape: a software
1063 environment for integrated models of biomolecular interaction networks. Genome Res
1064 13**:** 2498-2504.
1065 Standart, N., and N. Minshall, 2008 Translational control in early development: CPEB, P-bodies
1066 and germinal granules. Biochem Soc Trans 36**:** 671-676.
1067 Stepien, B. K., C. Oppitz, D. Gerlach, U. Dag, M. Novatchkova *et al.*, 2016 RNA-binding
1068 profiles of Drosophila CPEB proteins Orb and Orb2. Proc Natl Acad Sci U S A 113**:**
1069 E7030-E7038.
1070 Stoiber, M. H., S. Olson, G. E. May, M. O. Duff, J. Manent *et al.*, 2015 Extensive cross-
1071 regulation of post-transcriptional regulatory networks in Drosophila. Genome Res 25**:**
1072 1692-1702.
1073 Tadros, W., A. L. Goldman, T. Babak, F. Menzies, L. Vardy *et al.*, 2007 SMAUG is a major
1074 regulator of maternal mRNA destabilization in Drosophila and its translation is activated
1075 by the PAN GU kinase. Dev Cell 12**:** 143-155.
1076 Tadros, W., and H. D. Lipshitz, 2009 The maternal-to-zygotic transition: a play in two acts.
1077 Development 136**:** 3033-3042.
1078 Thomsen, S., S. Anders, S. C. Janga, W. Huber and C. R. Alonso, 2010 Genome-wide analysis
1079 of mRNA decay patterns during early Drosophila development. Genome Biol 11**:** R93.
1080 Vastenhouw, N. L., W. X. Cao and H. D. Lipshitz, 2019 The maternal-to-zygotic transition
1081 revisited. Development 146.
1082 Wang, X. P., and N. G. Cooper, 2009 Characterization of the transcripts and protein isoforms for
1083 cytoplasmic polyadenylation element binding protein-3 (CPEB3) in the mouse retina.
1084 BMC Mol Biol 10**:** 109.
1085 Warde-Farley, D., S. L. Donaldson, O. Comes, K. Zuberi, R. Badrawi *et al.*, 2010 The
1086 GeneMANIA prediction server: biological network integration for gene prioritization and
1087 predicting gene function. Nucleic Acids Res 38**:** W214-220.
1088 Whitten, D., 2011 Classification and clustering of sequencing data using a Poisson model, pp.
1089 2493-2518. Annals of Applied Statistics.
1090 Wilhelm, J. E., M. Hilton, Q. Amos and W. J. Henzel, 2003 Cup is an eIF4E binding protein
1091 required for both the translational repression of oskar and the recruitment of Barentsz. J
1092 Cell Biol 163**:** 1197-1204.
1093 Xu, S., N. Hafer, B. Agunwamba and P. Schedl, 2012 The CPEB protein Orb2 has multiple
1094 functions during spermatogenesis in Drosophila melanogaster. PLoS Genet 8**:** e1003079.
1095 Zavortink, M., L. N. Rutt, S. Dzitoyeva, J. C. Henriksen, C. Barrington *et al.*, 2020 The E2
1096 Marie Kondo and the CTLH E3 ligase clear deposited RNA binding proteins during the
1097 maternal-to-zygotic transition. Elife 9.

1098

1099 ## Figure Legends

1100 **Figure 1. RIP-seq identifies over 450 ORB2 targets in 0-3 hr embryos.** (a) Domain structure
1101 of ORB2B and location of the antigen used to screen for phage-displayed synthetic antibodies.
1102 (b) Scatterplot depicting the Log_2(Fold Enrichment)/Input Abundance (TPM) for all genes
1103 identified in the RIP-seq analysis; each point represents a single gene. Values represent the
1104 average enrichment from three independent biological replicates. ORB2 targets (red) are defined
1105 as having fold enrichment >1.5 in the anti-ORB2 RIP-seq compared to input and a ratio of
1106 ORB2/Control > 1.5, with an FDR adjusted *P*-value < 0.05; genes enriched in both ORB2 and
1107 control RIP-seq (green) are defined as having fold enrichment >1.5 in both anti-ORB2 and
1108 control RIP-seq, with a ratio of ORB2/Control < 1.5 and an FDR adjusted *P*-value < 0.05;
1109 Control enriched transcripts (blue) are defined as having fold enrichment <-1.5 in the control
1110 RIP-seq, fold enrichment < -1.5 in the anti-ORB2 RIP-seq, and an FDR adjusted *P*-value < 0.05.
1111 Dotted lines indicate ±1.5 fold-change thresholds. (c) Violin and boxplots depicting the
1112 distribution of transcript abundance as measured by average TPM from three biological
1113 replicates based on bound status as described in (A). Wilcoxon Rank Sum Test with Bonferroni
1114 multiple-test correction: ** = $P < 10^{-10}$; *** = $P < 10^{-15}$. (d) Validation of RIP-seq targets by RT-
1115 qPCR; bar graphs depict the log_2(fold enrichment) in an anti-ORB2 RIP-RT-qPCR compared to
1116 control RIP-RT-qPCR; *P*-values given are derived from Wilcoxon Signed Rank Test comparing
1117 ORB2 RIP-RT-qPCR to control RIP-RT-qPCR.

1118 **Figure 2. ORB2-bound transcripts are enriched in translationally repressed, unstable**
1119 **transcripts during the MZT.** Violin and boxplots depicting the relationship between ORB2-
1120 association and translational status, change in poly(A) tail length, and change in transcript
1121 abundance. Unbound genes include all expressed genes that were not defined as ORB2 targets in
1122 the RIP-seq analysis. (a) Translation efficiency, calculated from ribosome footprinting performed
1123 on 0-1 hour embryo extracts (EICHHORN *et al.* 2016). (b) Translation efficiency, calculated from
1124 ribosome footprinting performed on 2-3 hour embryo extracts (EICHHORN *et al.* 2016). (c)
1125 Translation efficiency as measured by ribosome profiling performed on 0-2 hour embryo extracts
1126 (DUNN *et al.* 2013). (d) Translation index, calculated from polysome gradients performed on 0-3
1127 hour embryo extracts (CHEN *et al.* 2014). (e) Change in transcript poly(A) tail length, calculated
1128 by comparing 0-1 hour and 2-3 hour embryo extracts, as measured by PAL-Seq (EICHHORN *et al.*
1129 2016). (f) Change in abundance, calculated by comparing 0-1 hour and 2-3 hour embryo extracts,
1130 as measured by RNA-Seq (EICHHORN *et al.* 2016). Wilcoxon Rank Sum Test: ** = $P < 10^{-10}$;
1131 *** = $P < 10^{-15}$.

1132 **Figure 3. ORB2 binding motifs predicted from RIP-seq confer translational repression on a**
1133 **reporter mRNA in S2 cells.** (a) ORB2 recognition element (ORE) enriched in ORB2 targets
1134 identified by *de novo* motif discovery using #ATS (LI *et al.* 2010) on results from the anti-ORB2
1135 RIP-seq in this study. (b) Diagram depicting the reporter Firefly Luciferase mRNA with six
1136 copies of different ORB2-binding motifs in the 3′UTR. (c) Bar graph depicting the enrichment of
1137 the luciferase reporter mRNA in an anti-ORB2 RIP-qPCR compared to Renilla Luciferase
1138 mRNA, normalized to a reporter without ORE motifs. Mutation of either the OREs or deletion of
1139 the RNA-binding domain (RRM) abrogate binding to the mRNA. (d) Bar graph depicting the
1140 ratio of luminescence between Firefly luciferase and Renilla luciferase. Mutation of either the
1141 OREs or deletion of the RNA-binding domain (RRM) abrogate repression. One-way ANOVA
1142 with Tukey multiple test correction: * = $P < 0.05$.

1143 **Figure 4. The ORB2 and hCPEB2 ZZ domain but not the ORB and hCPEB1 ZZ domain**
1144 **repress a luciferase reporter. (**a) Diagram depicting the tethering assay in which a polypeptide
1145 of interest fused to the BIV Tat domain is tethered to a Firefly luciferase reporter mRNA
1146 carrying six tandem repeat TAR elements in the 3′UTR. (b) Bar graph depicting the expression
1147 of the reporter firefly luciferase (normalized to co-transfected Renilla luciferase and normalized
1148 to steady state RNA levels) when tethering whole ORB2 or ORB2 fragments compared to GFP
1149 control. The ORB2 ZZ domain is necessary and sufficient for repression. (c) Bar graph depicting
1150 the expression of the reporter firefly luciferase mRNA measured by RT-qPCR (normalized to co-
1151 transfected Renilla luciferase mRNA) when tethering whole ORB2 or ORB2 fragments
1152 compared to GFP control. Reporter mRNA levels are unaffected by ORB2 ZZ or ORB2ΔZZ. (d)
1153 amino acid sequence alignment of the ZZ domains of ORB2, ORB, and their human orthologs,
1154 hCPEB1 and hCPEB2. The arrowhead denotes the junction between the RBD and ZZ domains.
1155 (e) Bar graph depicting the expression of the reporter firefly luciferase (normalized to co-
1156 transfected Renilla luciferase) when tethering different CPEB ZZ domains. Only ORB2 and
1157 hPEB2 repress. (f) Bar graph depicting the expression of the reporter firefly luciferase when
1158 ORB ZZ chimeric domains harboring substitutions from the ORB2 ZZ domain, are tethered. The
1159 ORB2 'A' and 'C' regions are each sufficient to convert the ORB ZZ domain into a repressor.
1160 One-way ANOVA with Hold-Sidak multiple test correction: * = $P < 0.05$; ** = $P < 0.001$; *** =
1161 $P < 10^{-5}$.

1162 **Figure 5. Anti-ORB2 IP-MS from early embryo extracts identifies known translation**
1163 **repressors and the PIC as binding partners.** (a) Interaction network depicting the connections
1164 between components of the Cup repressive complex and other translational repressors identified
1165 as ORB2 interactors by SAINT analysis. (b) Interaction network depicting the connections
1166 between components of eukaryotic PIC identified as ORB2 interactors by SAINT analysis.
1167 Interaction networks were produced by the GeneMANIA app for Cytoscape (FRANZ *et al.* 2018);
1168 size of node indicates average number of spectral counts obtained in the IP-MS; thickness of
1169 edges indicates strength of interaction assigned by GeneMANIA.

1170 **Figure 6. Deletion of the ORB2 ZZ domain results in derepression of target RNAs in the**
1171 **early embryo.** (a) Violin and boxplots comparing target and non-target abundance as determined
1172 by RNA-Seq in 0-1, 1-2 and 2-3 hour old embryos laid by w^{1118} and $orb2^{\Delta ZZ}$ females. No
1173 significant difference was detected for either genotype at any of the time-points. (b) Violin and
1174 boxplots comparing target and non-target translation index as determined by polysome gradients
1175 followed by RNA-Seq in 0-1, 1-2 and 2-3 hour old embryos laid by w^{1118} and $orb2^{\Delta ZZ}$ females.
1176 ORB2 targets were significantly derepressed in 0-1 hour old $orb2^{\Delta ZZ}$ embryos relative to w^{1118}.
1177 Log2(Ratio of mean normalized counts of pool 3 /mean normalized counts of pool 1 mean) was
1178 calculated for each transcript. Wilcoxon Rank Sum Test: ** = $P < 0.006$.

1179 ## Table Legends

1180 **Table 1. Overlap between the list of ORB2 targets and lists of genes associated with mRNA**
1181 **stability or decay in the early embryo.**

1182 **Table 2. Molecular Function GO-terms enriched in ORB2 targets.** GO-term analysis was
1183 performed using the gProfiler2 tool (KOLBERG *et al.* 2023).

1184 **Table 3. Biological Process GO-terms enriched in ORB2 targets.** GO-term analysis was
1185 performed using the gProfiler2 tool (KOLBERG *et al.* 2023).

1186 **Table 4. Cellular Component GO-terms enriched in ORB2 targets.** GO-term analysis was
1187 performed using the gProfiler2 tool (KOLBERG *et al.* 2023).

1188 Supplemental Figure Legends

1189 **Figure S1. Replicate-to-replicate comparisons of transcript TPMs from RIP-seq**
1190 **experiments show high correlation between replicates.** (a)-(c) Pairwise comparisons of three
1191 biological replicates performed with the anti-ORB2 E8 Fab. The Pearson correlation coefficient
1192 and its corresponding *P*-value were calculated and used to determine the degree of similarity
1193 between each pair. (d) Heatmap of the Poisson distance between three biological RIP-seq
1194 replicates performed with anti-ORB2 E8 Fab and three biological RIP-seq replicates performed
1195 with control C1 Fab. The Poisson distance is calculated by the difference in Poisson distribution
1196 between pairs of samples; a larger distance indicates a greater level of dissimilarity between
1197 samples.

1198 **Figure S2. Expression levels of ORB2, ORB2ΔRRM, and GFP in S2 cells.** Each set of three
1199 lanes corresponds to the ORE validation experiments in which expression vectors for tagged
1200 proteins and reporter mRNA constructs containing various recognition motifs were transfected
1201 into S2 cells, described in Figure 3.

1202 **Figure S3. Expression of ORB2 full-length protein, portions of ORB2, and the ZZ domains**
1203 **of ORB, ORB2, hPCPEB1 and 2 in S2 cells.** (a) Western blot showing the expression of ORB2
1204 full-length protein and protein portions corresponding to the experiments described in Figure 4b
1205 and c. (b) Western blot showing the expression of ORB2B and ORB2BΔZZ to the experiments
1206 described in Figure 4b and c. (c) Western blot showing the expression of ORB2 ZZ, hCPEB2
1207 ZZ, ORB ZZ and hCPEB1 ZZ corresponding to the experiments described in Figure 4e.

1208 **Figure S4. Structure of ZZ domains of CPEB family members.** (a) The NMR structure of the
1209 ZZ domain of human CPEB1 Protein Data Bank accession 2M13 (MERKEL *et al.* 2013) is
1210 shown, along with the Alphafold 3 (ABRAMSON *et al.* 2024) predicted structures of the ZZ
1211 domains of ORB, hCPEB2 and ORB2. The colors in the Alphafold 3 predictions represent the
1212 predicted local distance difference test (pLDDT) scores, where higher numbers indicate greater
1213 confidence in the prediction. (b) On the left is an overlap of the ORB and ORB2 predicted
1214 structures with Region A (the Rd turn), Region B (the beta hairpin), and Region C (the alpha
1215 helix) of each protein indicated. The boxes on the right highlight each region individually in two
1216 different orientations.

1217 **Figure S5. The predicted structures of chimeric ZZ domains.** Alphafold 3 (ABRAMSON *et al.*
1218 2024) predictions for chimeric ZZ domains where one of Regions A, B or C of ORB was
1219 replaced with the corresponding region from ORB2. The top row of images indicates the identity
1220 each construct as described in Figure 4f, while the bottom row shows the pLDDT scores for each
1221 prediction.

1222 **Figure S6. Expression of chimeric ORB-ORB2 ZZ domain proteins in S2 cells.** Western blot
1223 showing the expression of ORB-ORB2 chimeric proteins corresponding to the substitution

1224 experiments which assessed transformation of the non-repressing ORB ZZ domain into a
1225 translational repressor, as shown in Figure 4f.

1226 **Figure S7. CRISPR Cas9-mediated endogenous deletion of the ORB2 ZZ domain was used**
1227 **to generate *orb2*$^{\Delta ZZ}$ flies.** (a) Diagram depicting the *orb2* endogenous locus, located at 66E4-
1228 66E5 on 3L, the corresponding mRNAs that are encoded, and the targeted deletion. (b) Agarose
1229 gel of the PCR amplification of the region surrounding the CRISPR targeted deletion of the F1
1230 generation post-injection. Genotypes indicate lines generated from individual F1 flies. Up PCR
1231 indicates PCR amplification using primers designed against the 5′ insertion junction; Down PCR
1232 indicates PCR amplification using primers designed against the 3′ insertion junction. (c) Agarose
1233 gel of the PCR amplification of the region surrounding the PiggyBac transposon-mediated
1234 excision of the dsRed marker. WT indicates the band representing PCR amplification of the
1235 endogenous ORB2 locus containing an intact ZZ domain; Excised indicates the band
1236 representing amplification of the locus with the ZZ domain deletion without the dsRed marker.
1237 Genotypes indicate lines generated from individual flies resulting from the CRISPR injection. (d)
1238 Western blot showing expression of endogenous ORB2 and CRISPRed ORB2ΔZZ in
1239 heterozygous and homozygous whole flies. ORB2ΔZZ is expressed at higher levels than full-
1240 length ORB2 (see heterozygote for comparison). Generation of CRISPR mutants was performed
1241 by WellGenetics as described in the Materials and Methods.

1242 **Figure S8. ORB2ΔZZ retains RNA-binding to its targets in embryos.** (a) Western blot
1243 showing the expression of ORB2 and ORB2ΔZZ protein over the first four hours of embryonic
1244 development. (b) Bar graph depicting the enrichment of five ORB2 target mRNAs in RIP-RT-
1245 qPCR from 0-3 hour old embryos laid by w^{1118} and *orb2*$^{\Delta ZZ}$ females. The ORB2 RIPs used the
1246 ORB2 E8 Fab; the control RIP used the C1 Fab. RNA levels were normalized to *RpL32* mRNA.
1247 n = 3; error bars are standard deviation. Student's *t*-test *P*-values were not significant (n.s.; $P >$
1248 0.05)

1249 Supplemental File Legends

1250 **File S1. Results of RIP-seq of ORB2 in 0-3 hour embryos.** See Materials and Methods for
1251 details.

1252 **File S2. Results of *de novo* motif discovery on ORB2 targets in 0-3 hour embryos.** Motif
1253 discovery was carried out using #ATS as described (Li *et al.* 2010). See Materials and Methods
1254 for details.

1255 **File S3. Results of IP-MS of ORB2 and ORB2ΔZZ in 0-3 hour embryos in the presence or**
1256 **absence of RNase A.** Interactors were identified using SAINT as described (Choi *et al.* 2012).
1257 See Materials and Methods for details.

1258 **File S4. Lists of mRNAs bound by ORB2 (RIP-seq) whose protein products were also**
1259 **identified as interactors in ORB2 IP-MS.**

1260 **File S5. Results of RNA-seq time-course in wild-type and ORB2ΔZZ embryos.** See Materials
1261 and Methods for details.

1262 **File S6. Results of polysome gradient RNA-seq time-course in wild-type and ORB2ΔZZ**
1263 **embryos.** See Materials and Methods for details.

FIGURE 1

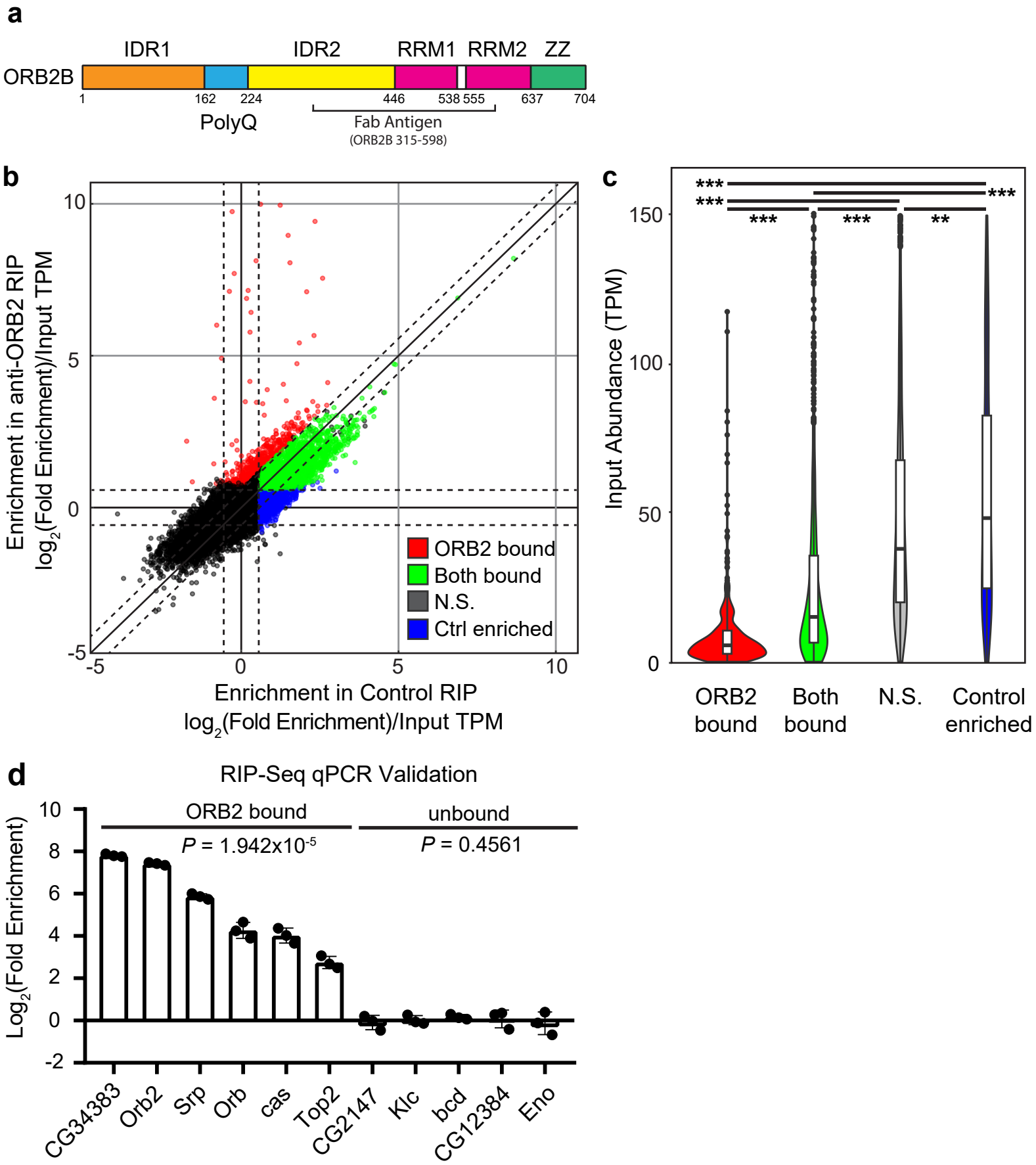
a
IDR1
IDR2
RRM1
RRM2
ZZ
ORB2B
1
162
224
446
538
555
637
704
PolyQ
Fab Antigen
(ORB2B 315-598)
b
Enrichment in anti-ORB2 RIP
log2(Fold Enrichment)/Input TPM
Enrichment in Control RIP
log2(Fold Enrichment)/Input TPM
ORB2 bound
Both bound
N.S.
Ctrl enriched
c
Input Abundance (TPM)
ORB2 bound
Both bound
N.S.
Control enriched
d
RIP-Seq qPCR Validation
ORB2 bound
unbound
P = 1.942x10-5
P = 0.4561
Log2(Fold Enrichment)
CG34383
Orb2
Srp
Orb
cas
Top2
CG2147
Klc
bcd
CG12384
Eno

FIGURE 2

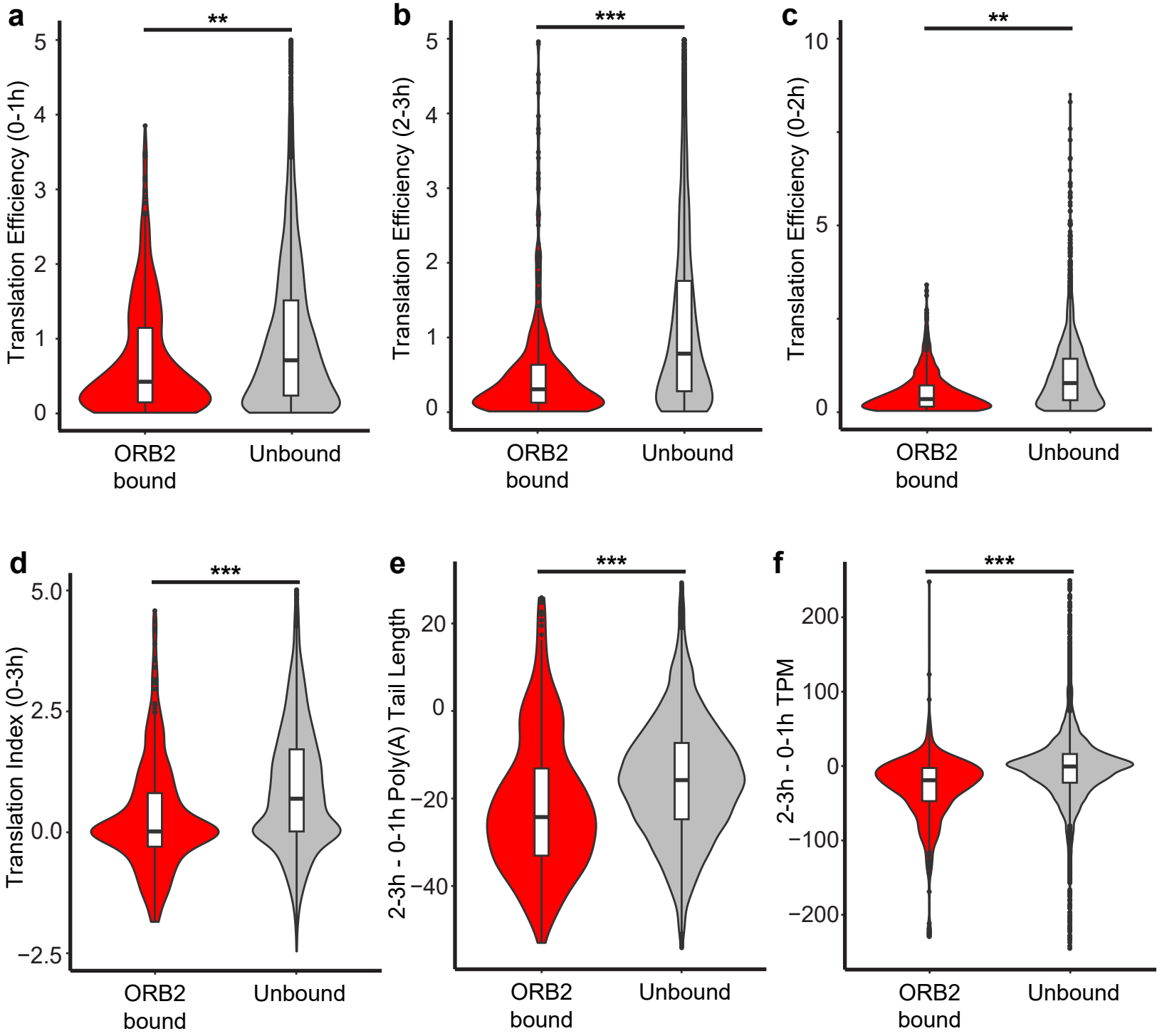
a
**
Translation Efficiency (0-1h)
5
4
3
2
1
0
ORB2 bound
Unbound
b
***
Translation Efficiency (2-3h)
5
4
3
2
1
0
ORB2 bound
Unbound
c
**
Translation Efficiency (0-2h)
10
5
0
ORB2 bound
Unbound
d
***
Translation Index (0-3h)
5.0
2.5
0.0
−2.5
ORB2 bound
Unbound
e
***
2-3h - 0-1h Poly(A) Tail Length
20
0
−20
−40
ORB2 bound
Unbound
f
***
2-3h - 0-1h TPM
200
100
0
−100
−200
ORB2 bound
Unbound

FIGURE 3

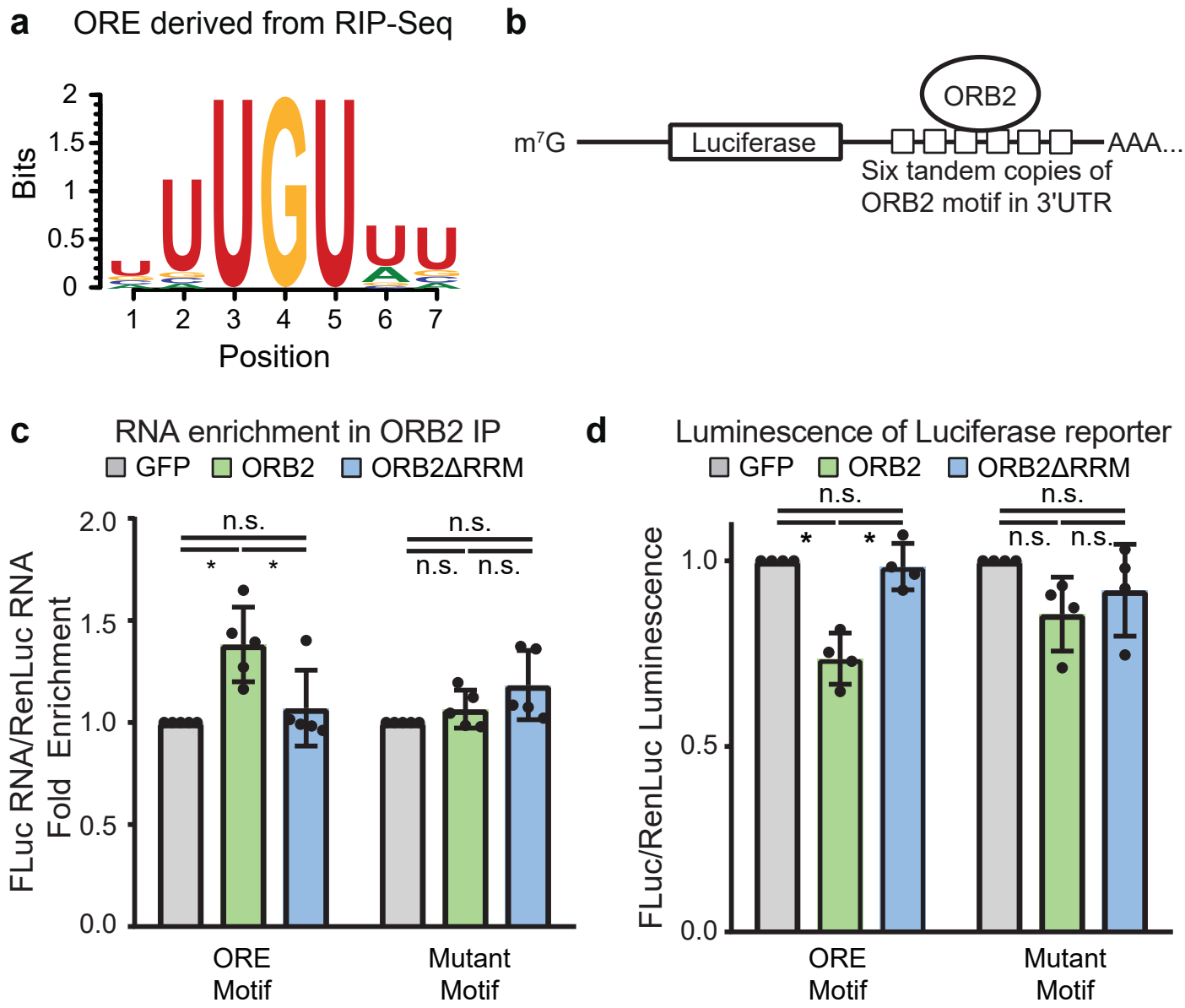
a
ORE derived from RIP-Seq
Bits
2
1.5
1
0.5
0
1 2 3 4 5 6 7
Position
b
ORB2
m7G
Luciferase
AAA...
Six tandem copies of
ORB2 motif in 3'UTR
c
RNA enrichment in ORB2 IP
GFP
ORB2
ORB2ΔRRM
FLuc RNA/RenLuc RNA
Fold Enrichment
2.0
1.5
1.0
0.5
0.0
n.s.
*
*
n.s.
n.s.
n.s.
ORE
Motif
Mutant
Motif
d
Luminescence of Luciferase reporter
GFP
ORB2
ORB2ΔRRM
FLuc/RenLuc Luminescence
1.0
0.5
0.0
n.s.
*
*
n.s.
n.s.
n.s.
ORE
Motif
Mutant
Motif

FIGURE 4

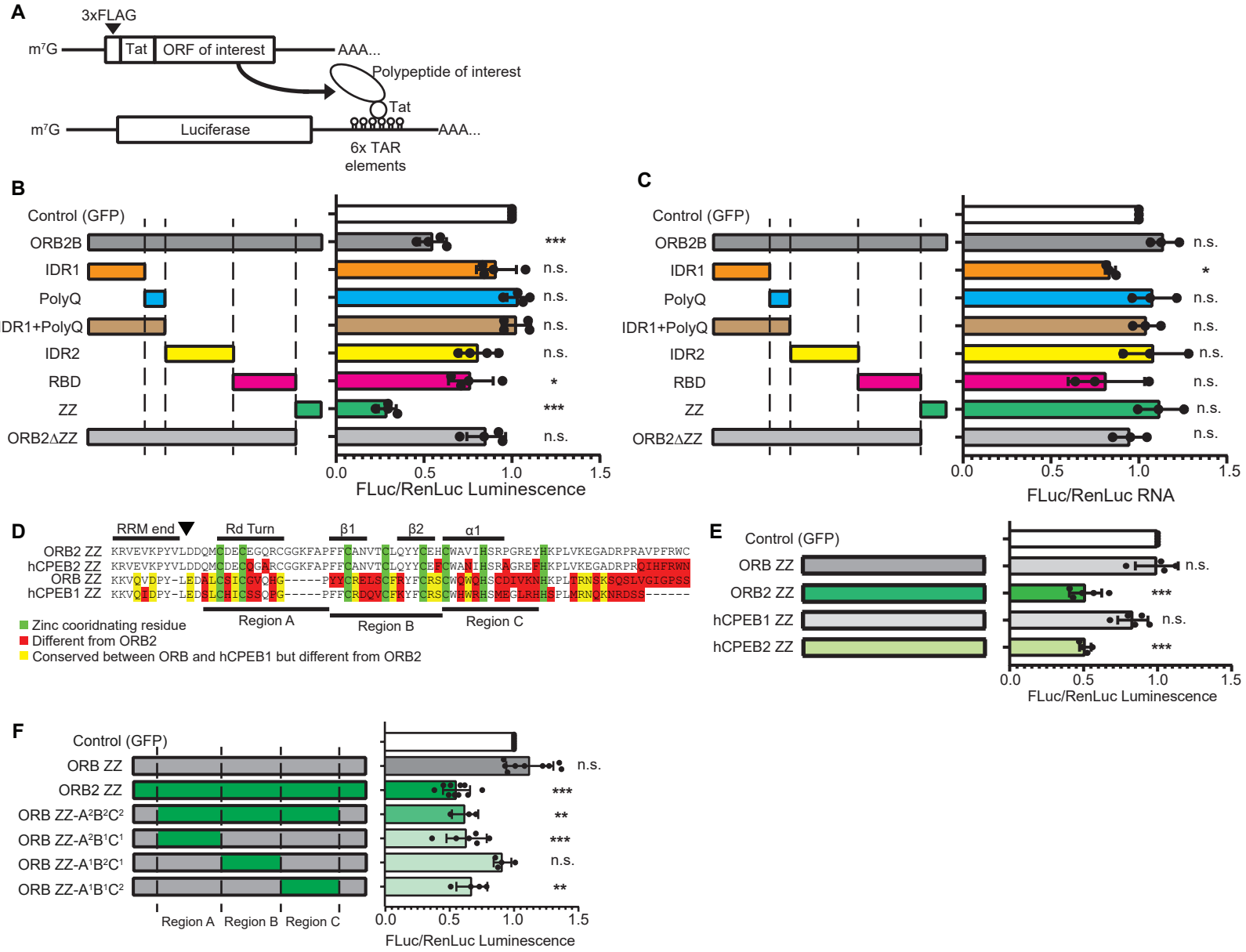
A
3xFLAG
m7G
Tat
ORF of interest
AAA...
Polypeptide of interest
Tat
m7G
Luciferase
AAA...
6x TAR elements
B
Control (GFP)
ORB2B
IDR1
PolyQ
IDR1+PolyQ
IDR2
RBD
ZZ
ORB2ΔZZ
***
n.s.
n.s.
n.s.
n.s.
*
***
n.s.
0.0
0.5
1.0
1.5
FLuc/RenLuc Luminescence
C
Control (GFP)
ORB2B
IDR1
PolyQ
IDR1+PolyQ
IDR2
RBD
ZZ
ORB2ΔZZ
n.s.
*
n.s.
n.s.
n.s.
n.s.
n.s.
n.s.
0.0
0.5
1.0
1.5
FLuc/RenLuc RNA
D
RRM end
Rd Turn
β1
β2
α1
ORB2 ZZ
hCPEB2 ZZ
ORB ZZ
hCPEB1 ZZ
Region A
Region B
Region C
Zinc cooridnating residue
Different from ORB2
Conserved between ORB and hCPEB1 but different from ORB2
E
Control (GFP)
ORB ZZ
ORB2 ZZ
hCPEB1 ZZ
hCPEB2 ZZ
n.s.
***
n.s.
***
0.0
0.5
1.0
1.5
FLuc/RenLuc Luminescence
F
Control (GFP)
ORB ZZ
ORB2 ZZ
ORB ZZ-A2B2C2
ORB ZZ-A2B1C1
ORB ZZ-A1B2C1
ORB ZZ-A1B1C2
n.s.
***
**
***
n.s.
**
Region A
Region B
Region C
0.0
0.5
1.0
1.5
FLuc/RenLuc Luminescence

FIGURE 5

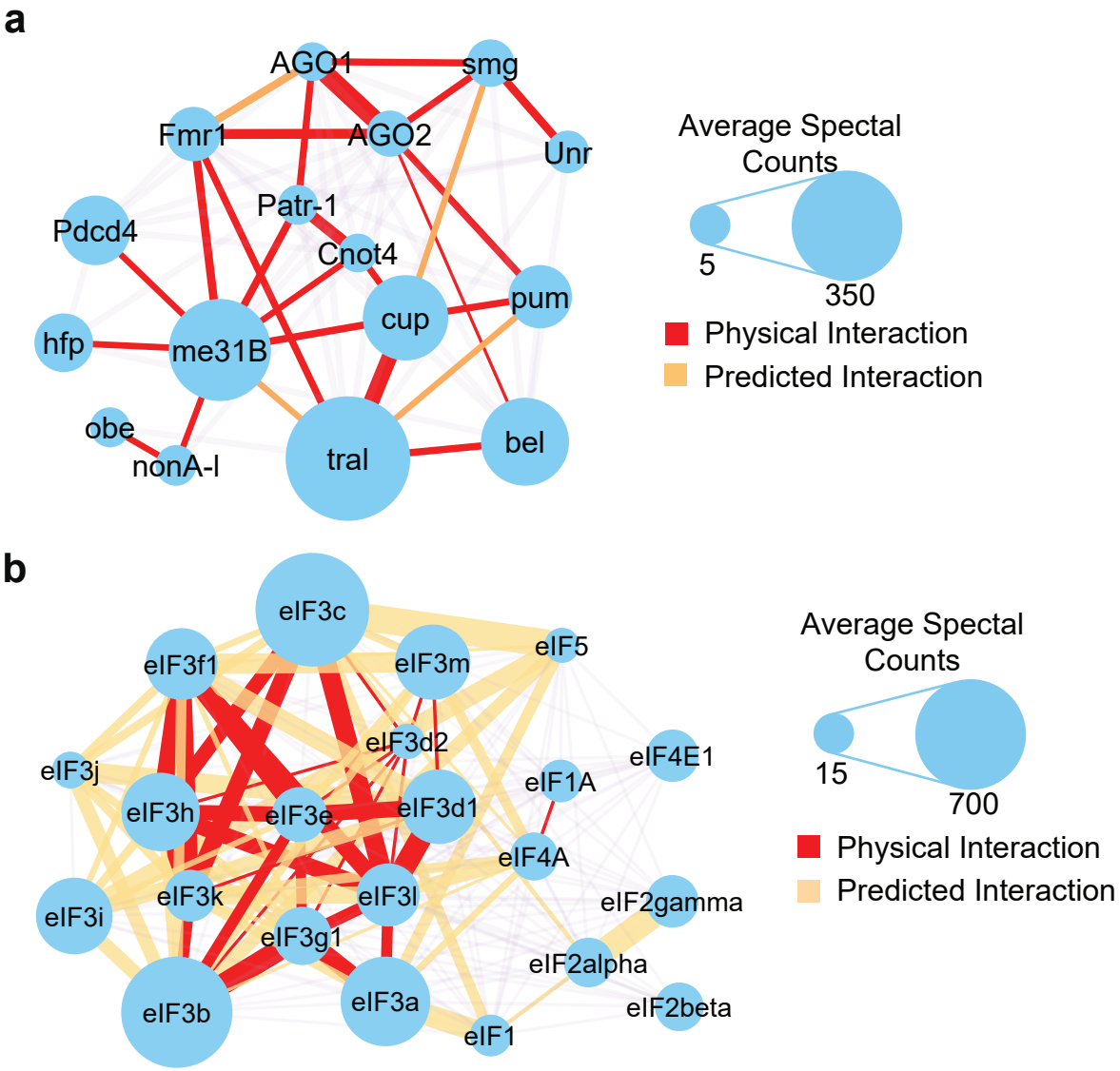
a
AGO1
smg
Fmr1
AGO2
Unr
Patr-1
Pdcd4
Cnot4
pum
cup
hfp
me31B
obe
nonA-I
tral
bel
Average Spectal Counts
5
350
Physical Interaction
Predicted Interaction
b
eIF3c
eIF3f1
eIF3m
eIF5
eIF3d2
eIF4E1
eIF3j
eIF1A
eIF3h
eIF3e
eIF3d1
eIF4A
eIF3k
eIF3l
eIF2gamma
eIF3i
eIF3g1
eIF2alpha
eIF3b
eIF3a
eIF2beta
eIF1
Average Spectal Counts
15
700
Physical Interaction
Predicted Interaction

FIGURE 6

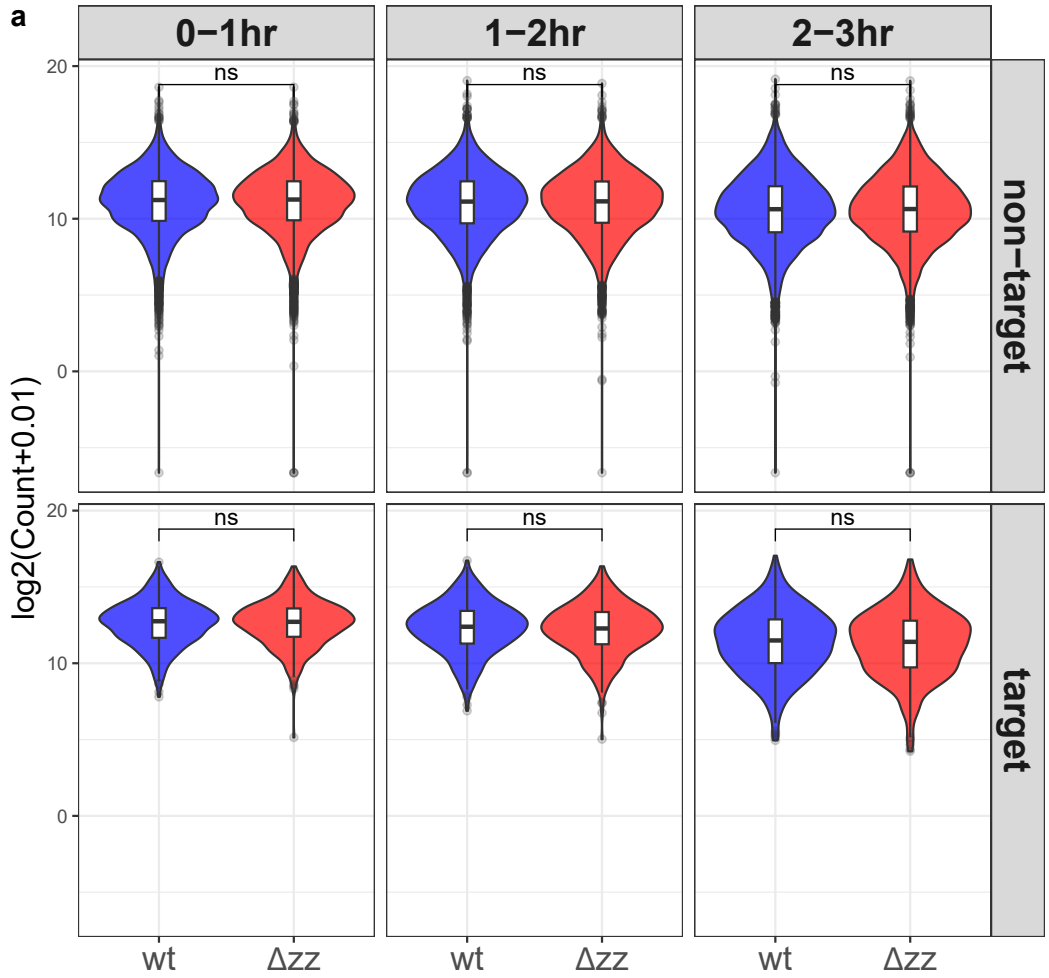
a
0−1hr
1−2hr
2−3hr
non−target
target
log2(Count+0.01)
ns
20
10
0
wt
Δzz

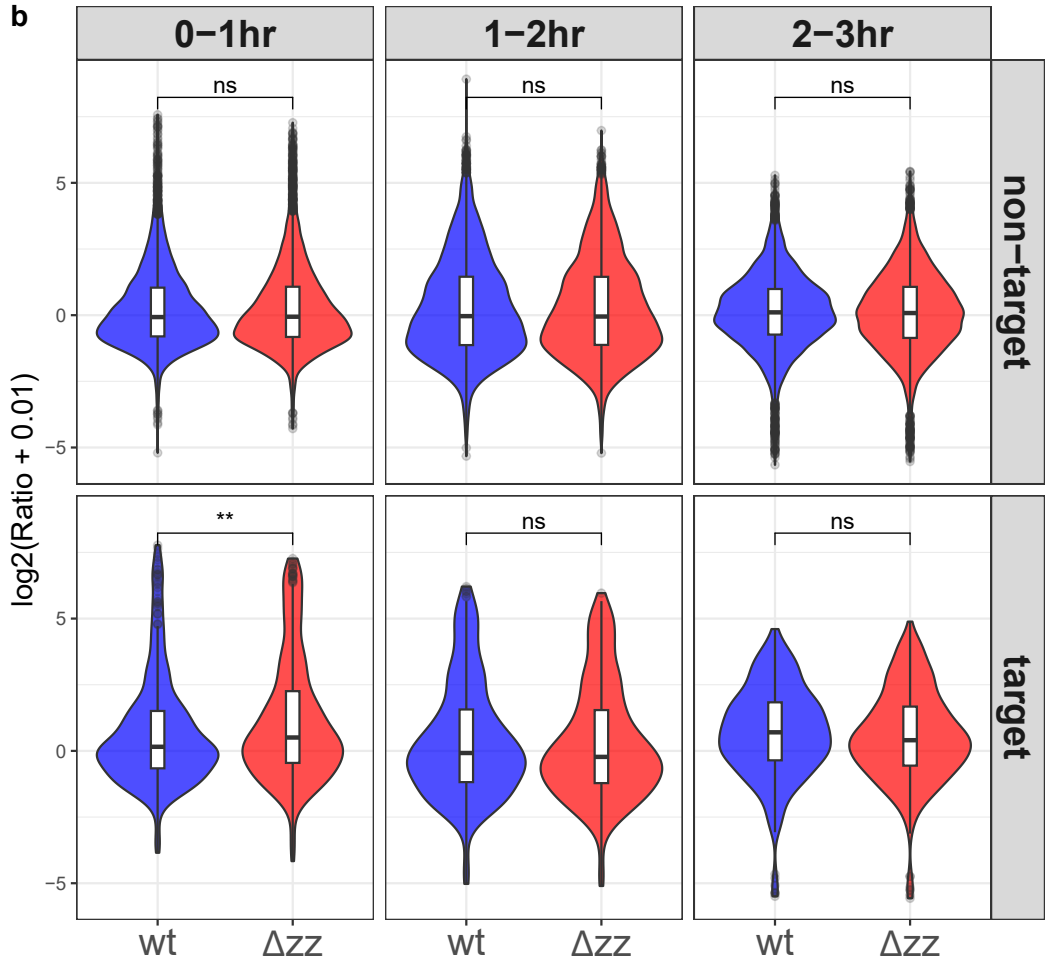
b
0−1hr
1−2hr
2−3hr
non−target
target
log2(Ratio + 0.01)
ns
**
5
0
−5
wt
Δzz

TABLE 1

Comparison	Backgound (Total)	Orb2 Only	Other Only	Overlap	Fisher's Exact p-value	Odds Ratio
Maternal Unstable (Unfertilized eggs, Tadros et al 2007)	3030	172	744	166	2.20E-16	3.849738
Thomsen et al 2010						
Class I (Stable transcripts)	4186	377	1335	35	2.20E-16	0.2334165
Class II (Maternal Decay only)	5108	395	394	36	0.3359	1.181531
Class III (Maternal Decay + Transcription)	5177	392	326	38	0.02109	1.539281
Class IV (Zygotic Decay only)	4332	322	1171	108	0.06763	1.240746
Class V (Both Maternal + Zygotic Decay)	4186	239	1317	191	2.20E-16	2.53962

TABLE 2. Molecular Function

GO Term Name	Adjusted p-value	GO Term Size	ORB2 targets	Overlap
protein binding	1.13E-21	3760	416	229
mRNA 3'-UTR binding	5.78E-11	48	416	17
mRNA binding	1.15E-10	238	416	35
mRNA regulatory element binding translation repressor activity	2.51E-08	18	416	10
translation repressor activity	7.18E-08	25	416	11
translation regulator activity	2.28E-04	106	416	16
catalytic activity, acting on DNA	2.49E-04	147	416	19
protein serine/threonine kinase activity	5.25E-04	184	416	21
DNA binding	6.42E-04	1127	416	69
poly-pyrimidine tract binding	1.28E-03	14	416	6
adenyl ribonucleotide binding	1.42E-03	846	416	55
catalytic activity, acting on a nucleic acid	1.62E-03	406	416	33
ATP binding	2.44E-03	840	416	54
purine ribonucleotide binding	2.99E-03	1021	416	62
purine nucleotide binding	3.63E-03	1072	416	64
adenyl nucleotide binding	3.73E-03	896	416	56
ribonucleotide binding	4.31E-03	1033	416	62

TABLE 3. Biological Process

GO Term Name	adjusted p-value	GO Term Size	ORB2 targets	Overlap
purine ribonucleoside triphosphate binding	4.48E-03	1012	416	61
anatomical structure development	5.77E-28	2775	435	212
developmental process	2.30E-27	2954	435	219
negative regulation of cellular process	1.73E-25	1520	435	144
cell development	6.92E-25	1450	435	139
multicellular organism development	8.26E-25	2276	435	182
cell differentiation	3.46E-24	1768	435	155
cellular component organization	1.07E-21	3178	435	217
regulation of metabolic process	1.81E-21	2253	435	174
gamete generation	1.19E-20	917	435	100
germ cell development	7.67E-20	721	435	86
anatomical structure morphogenesis	1.34E-19	1580	435	136
oogenesis	1.45E-19	582	435	76
system development	5.09E-19	1527	435	132
multicellular organismal reproductive process	1.60E-18	1096	435	107
regulation of primary metabolic process	1.69E-17	1860	435	146
nervous system development	4.18E-17	1196	435	110
animal organ development	5.43E-17	1200	435	110
regulation of macromolecule biosynthetic process	1.09E-15	1742	435	136

TABLE 4. Cellular Component

GO Term Name	adjusted p-value	GO Term Size	ORB2 targets	Overlap
nucleus	1.99E-14	3234	438	196
ribonucleoprotein granule	2.57E-12	119	438	27
cytoplasmic ribonucleoprotein granule	7.11E-12	114	438	26
cellular anatomical structure	6.48E-10	10708	438	426
cytoplasm	6.02E-09	5187	438	255
P granule	1.14E-07	46	438	14
cytosol	1.14E-07	1131	438	82
germ plasm	2.15E-07	48	438	14
nucleoplasm	1.40E-06	573	438	50
pole plasm	2.54E-06	57	438	14
nuclear lumen	3.31E-06	910	438	67
cytoplasmic stress granule	5.07E-06	21	438	9
protein-containing complex	2.53E-05	2861	438	151
chromosome	3.50E-05	787	438	58
PcG protein complex	8.68E-04	27	438	8
transferase complex	2.13E-03	550	438	41
intracellular protein-containing complex	4.15E-03	625	438	44
cell junction	4.67E-03	608	438	43
intracellular organelle lumen	4.94E-03	1158	438	69
membrane-enclosed lumen	5.08E-03	1159	438	69
organelle lumen	5.08E-03	1159	438	69
cell cortex	5.36E-03	208	438	21